https://doi.org/10.1016/j.applthermaleng.2020.115093


# Experimental and theoretical analysis of functional controllability for multi-condenser heat pumps

Zi-Yang Zhang[a,b], Chun-Lu Zhang[a,*], Fu Xiao[b]

[a]*Institute of Refrigeration and Cryogenics, School of Mechanical Engineering, Tongji University, Shanghai, China*

[b]*Research Institute for Sustainable Urban Development, The Hong Kong Polytechnic University, Hong Kong, China*

## Abstract

Multi-split air conditioning systems are finding increasing applications in both residential and commercial buildings. Control of multi-split air conditioning systems have received considerable attentions. Most studies have focused on control methods for the cooling mode, while very few control methods have been developed for the heating mode. A widely adopted heating control strategy for a typical multi-condenser heat pump is regulating the indoor electronic expansion valve (EXV) openings to control subcooling or supply air temperature of each indoor unit and simultaneous regulating the outdoor EXV opening to control suction superheat. We found from experimental study that this control strategy may cause unstable EXV openings and poor command-following performance. By performing functional controllability analysis, we provide a theoretical insight into the uncontrollable problem and prove that the system is functionally uncontrollable when the conventional heating control strategy is used. Based on findings from functional controllability analysis, a modified system configuration is proposed, with a refrigerant receiver added between the indoor EXVs and the outdoor EXV. The new system proves to be functionally controllable. Moreover, simulated command-following controllability tests show that the modified system has better performance. This paper verified the ability of functional controllability analysis in detecting structural control problems for refrigeration systems, which can be used as a general method for practical applications.

**Keywords**: Multi-split heat pump; Control; Functional controllability; Dynamic modeling;

* Corresponding author. Tel.: +86-136-71825-133.

*E-mail address*: chunlu.zhang@gmail.com (C.-L. Zhang)

**Nomenclature**

| | |
|---|---|
| $A$ | area ($m^2$) |
| $A_1$ | flow area of indoor EXV 1 ($m^2$) |
| $A_2$ | flow area of indoor EXV 2 ($m^2$) |
| $A_d$ | flow area of outdoor EXV ($m^2$) |
| $A_r$ | area ratio |
| $c_p$ | specific heat at constant pressure (kJ $kg^{-1}$ $K^{-1}$) |
| D | diameter (m) |
| $f$ | compressor speed (rps) |
| **G**(s) | transfer function |
| $H$ | height (m) |
| $h$ | specific enthalpy (kJ $kg^{-1}$) |
| $I$ | identity matrix |
| $k$ | partial derivative |
| $L$ | tube length (m) |
| $M$ | mass (kg) |
| $m$ | mass flow rate (kg $s^{-1}$) |
| $p$ | pressure (kPa) |
| $Q$ | heat transfer capacity (W) |
| $s$ | frequency |
| SP | setpoint |
| $T$ | temperature (°C, K) |
| $t$ | time |
| $W$ | power consumptions (W) |
| $z$ | length coordinate (m) |

**Greek symbol**

| | |
|---|---|
| $\alpha$ | heat transfer coefficient (W $m^{-2}$ $K^{-1}$) |
| $\varepsilon$ | emissivity |
| $\rho$ | density (kg $m^{-3}$) |
| $\gamma$ | void fraction |
| $\sigma$ | Stefan-Boltzmann constant |

**Superscript**

| | |
|---|---|
| dot | the first derivative of the marked parameter with respect to time |

**Subscript**

| | |
|---|---|
| a | air |
| c | condensing |
| c1 | desuperheating region of the condenser |
| c2 | two-phase region of the condenser |
| c3 | subcooling region of the condenser |
| ca | air flowing through the condenser |
| ci | condenser inlet |
| cint1 | saturated gas cross-section of the condenser |
| cint2 | saturated liquid cross-section of the condenser |
| co | condenser outlet, tube outside of the condenser |
| comp | compressor |
| cw | tube wall of the condenser |
| DB | dry bulb |
| d | discharge, downstream |
| d-exv | downstream expansion valve |
| dsh | discharge superheat |
| e | evaporating |
| e1 | two-phase region of the evaporator |
| e2 | superheated region of the evaporator |
| ea | air flowing through the evaporator |
| ei | evaporator inlet |
| eint | saturated gas cross-section of the evaporator |
| eo | evaporator outlet, tube outside of the evaporator |
| exv | electronic expansion valve |
| ew | tube wall of the evaporator |
| g | saturated gas |
| gc | saturated gas at the condensing pressure |
| ge | saturated gas at the evaporating pressure |

| | |
|---|---|
| l | saturated liquid |
| lc | saturated liquid at the condensing pressure |
| le | saturated liquid at the evaporating pressure |
| liq | subcooled liquid refrigerant leaving the condenser |
| m | intermediate |
| r | refrigerant |
| ri | receiver inlet |
| ro | receiver outlet |
| s | suction |
| sc | subcooling |
| sh | suction superheat |
| u | upstream |
| u-exv | upstream expansion valve |
| w | wall |
| WB | wet bulb |
| x0 | length coordinate where the refrigerant quality equals 0 |
| x1 | length coordinate where the refrigerant quality equals 1 |

# 1 Introduction

Multi-split air conditioning systems, also called as variable refrigerant flow (VRF) systems, consist of one outdoor unit and multiple indoor units. They have advantages over conventional air conditioning systems in energy efficiency and indoor thermal comfort [1]. Since they were first proposed in the 1980s, multi-split air conditioning systems have found increasing applications in both residential and commercial buildings. Control is crucial for the reliable and efficient operation of VRF systems and it presents a significant challenge because multiple refrigerant-to-air indoor units are strongly coupled and the cooling/heating loads differ for each indoor unit. Extensive research has therefore been conducted on the control of multi-split refrigeration and heat pump systems.

Most studies in the field focus on control methods for the cooling mode. Shah et al. [2] designed a linear quadratic regulator (LQR) for a dual-evaporator system based on its linearized dynamic model. Chen et al. [3] applied a self-tuning fuzzy control algorithm to control a triple-evaporator air conditioner. Elliott and Rasmussen [4] proposed a decentralized control structure for multi-evaporator vapor compression systems using model predictive control (MPC). Elliott and Rasmussen [5] further incorporated a supervisory controller to seek optimal set points of cooling capacity for local controllers. Lin and Yeh [6] investigated a cascade algorithm for refrigerant distribution between multiple evaporators. A mode-switching control method for dual-evaporator air conditioning systems was introduced by Lin and Yeh [7], in which switching between various operation combinations of indoor units was achieved by raising the temperature settings for the turned-off indoor units. Tu et al. [8] proposed to use the average suction pressure in an adjustment period, rather than the suction pressure at each moment, to regulate the output capacity of the digital scroll compressor of multi-split air conditioners. Xu et al. [9] developed and validated a novel capacity-modulation algorithm for a multi-evaporator system, in which the compressor speed regulated the overall cooling capacity and the indoor EXV openings controlled the corresponding indoor air temperature. Yun et al. [10] developed a load-responsive method to control the evaporating temperature in a VRF system for cooling energy savings. Matsumoto et al. [11] numerically analyzed the control characteristics of the indoor fan speed and expansion valve openings of a VRF system.

Very few studies have examined control methods for the heating mode. Tai [12] introduced a controller design process for multi-condenser heat pump systems, in which the compressor speed controls the total heating capacity and the indoor and outdoor expansion valves (EXV) control subcooling and suction superheat, respectively. Each single-input single-output (SISO)

control loop adopts the proportional-integral (PI) algorithm. Lee et al. [13] designed multi-input multi-output MIMO (PI) controllers for a multi-condenser heat pump system. The gains of the PI controllers were optimized using genetic algorithm (GA). They found that use of the optimized MIMO controller resulted in smaller overshoots and shorter settling time than the use of the SISO controller. Yun et al. [14] applied the load-responsive dynamic target high-pressure control method in a VRF system for heating energy savings. Moon et al. [15] developed a cost-effective control algorithm for VRF heating system, for which an artificial neural network model was used to determine the optimal operation parameters.

The aforementioned research concentrated on applying advanced control algorithms such as GA, MPC, and LQR to multi-split refrigeration or heat pump systems. Actually, control structure and control algorithm are two primary aspects in controller design, while the former plays the fundamental role. The control structure is related to the selection of variables to be measured and variables to be manipulated and how these variables get paired together [16]. This paper will focus on the control structure research for multi-split air conditioning systems.

A typical multi-split air conditioning system functional in both cooling and heating modes is depicted in Fig.1 [17-20]. According to existing researches and information from leading manufacturers, the widely adopted control structure for VRF system functions as follows. In the cooling mode, the indoor EXV openings and compressor speed are normally selected as manipulated variables, whereas the corresponding controlled outputs are supply air temperature/refrigerant superheat of each indoor unit and the suction pressure/total cooling capacity [3, 6-8, 21]. Note that the outdoor EXV is fully open in the cooling mode. In the heating mode, the compressor speed controls the discharge pressure to regulate total heating capacity. The indoor EXVs regulate refrigerant subcooling or supply air temperature to distribute the refrigerant mass flow rates among the indoor units. The outdoor EXV controls proper refrigerant superheat at the compressor suction port [12, 20-24]. The aforementioned control strategy has wide applications in industry and academia, and is referred to as the conventional control strategy in this study.

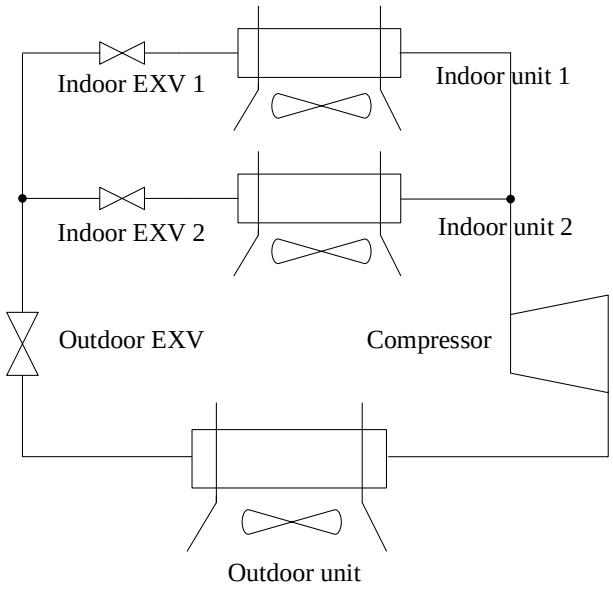


Fig.1 Schematic of a multi-split refrigeration/heat pump system

Comparing the control strategies for the heating mode and for the cooling mode, in addition to the different control targets of the indoor EXVs (i.e., subcooling and superheat, respectively), there is one more control loop in the heating mode, that is, control of the compressor suction superheat by regulation of the outdoor EXV. Such differences are caused by different roles which the indoor heat exchangers play in the two modes. In the cooling mode, indoor heat exchangers function as evaporators. By controlling superheat at the outlet of each evaporator, two control objectives, i.e., refrigerant flow distribution among indoor units and safe operation of the compressor can be simultaneous satisfied. In the heating mode, in contrast, indoor heat exchangers work as condensers. Flow distributions are achieved by controlling subcooling or supply air temperature of each indoor unit. Thereby, one more control loop., i.e. suction superheat regulated by outdoor EXV is needed to prevent liquid droplet from entering the compressor. However, because both indoor and outdoor EXVs control-loops influence the refrigerant mass flow rates in the heating mode, there is a risk that the indoor and outdoor EXVs control loops will interfere with each other and consequently the EXV openings are difficult to stabilize. This problem has never been investigated even discovered because previous related work [20, 24, 25] focused mainly on system energy efficiency, and impact of this control problem to energy efficiency is not apparent. However, the conventional strategy does cause frequent changes in EXV openings and therefore could weaken the system stability and reliability. This study aims to investigate the control performance of the abovementioned control structure in the heating mode.

The rest of the paper is organized as follows. Section 2 presents the experimental investigation of the performance of the conventional control strategy for the multi-condenser heat pump. Section 3 conducts theoretical analysis on the functional controllability of multi-condenser heat pumps, based on the dynamic physical model of a two-condenser heat pump developed and validated in this study. Section 4 proposes a modified system configuration and a novel control strategy. The command-following performance of the modified system under the novel control strategy is compared with that of the conventional system in simulation tests. Section 5 summarizes the conclusions and major contributions of this study.

# 2 Experimental investigation of control performance with conventional control strategy

In this section, the control performance of two multi-condenser heat pumps with the conventional strategy was experimentally investigated. The experimental results were analyzed based on system operation principles.

## 2.1 Case 1

In case 1, the dynamic behavior of a commercial multi-split air conditioning system was tested in the heating mode. The system consists of one outdoor unit and five indoor units, as shown in Fig. 2(a) and Fig. 2(b), with a rated heating capacity of 69 kW. Five indoor units are of identical size and capacity. Working fluid is R410A. It was tested in a psychrometric room comprising one indoor chamber and one outdoor chamber. The environmental chambers were conditioned by built-in air-conditioning systems to maintain the preset temperature and humidity. A schematic of the experimental setup and major sensors is depicted in Fig.2(c). The parameters to be measured were the refrigerant temperatures and pressures at the compressor suction and discharge ports, the refrigerant temperatures and pressures entering and exiting each indoor unit, the refrigerant temperatures entering and exiting the outdoor unit, and the dry bulb and wet bulb temperatures in the environmental chambers. The measurement instruments and their corresponding measuring accuracy are summarized in Table 1.

(a) Outdoor chamber (b) Indoor chamber

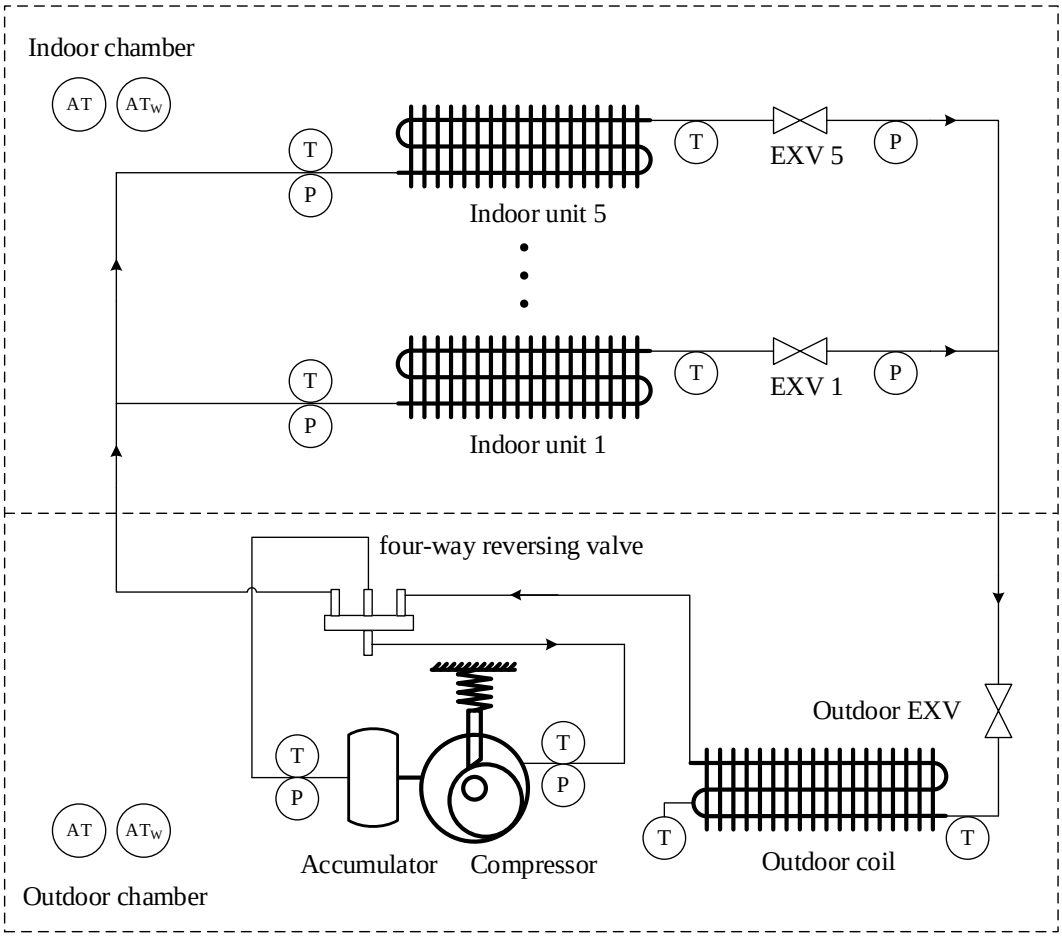


(c) Schematic of experimental setup

(T – refrigerant temperature; P – refrigerant pressure; AT – air dry bulb; $AT_W$ – air wet bulb)

Fig.2 Test facility of case 1

Table 1 Summary of measuring instruments

| Instrument | Sensor | Range | Accuracy |
|---|---|---|---|

| | | | |
|---|---|---|---|
| Thermal resistance | PT100 Class AA | -20–70 ºC | ± 0.1 °C |
| Thermal couple | T type | -20–70 ºC | ± 0.5 °C |
| Hygrometer | SHT30 | 0–70 ºC | ± 0.5 °C |
| Pressure transmitter | AP401 | 0–5000 kPa | ± 0.25 % F.S.* |

* F.S. stands for full scale.

The outdoor EXV and indoor EXVs are used to control suction superheat and subcooling, respectively. A case involving only one indoor unit being switched on was designed to study the interference between the indoor and outdoor EXV control loops. Testing conditions were $T_{DB}$ = 10 °C, $T_{WB}$ = 9 °C in the outdoor chamber, and $T_{DB}$ = 24 °C in the indoor chamber. The outdoor conditions are selected to avoid frosting.

Fig.3 depicts the dynamic response of some key parameters 30 min after start-up. As shown in Fig.3(a), the saturated suction and discharge temperature were almost stable at this time. However, Fig.3(b) shows that refrigerant suction superheat continuously increases, while the subcooling decreases contrarily. This result may be explained by the fact that the measured superheat was smaller than the control target, hence the outdoor EXV openings decreased in response. As the EXV openings of this commercial VRF unit cannot be directly measured, the decreasing outdoor EXV openings can be inferred from the increasing pressure drop through it as shown in Fig.3(c). The decreasing outdoor EXV openings led to a lower refrigerant mass flow rate and thereby greater subcooling, probably to degree larger than the control target. Reactively, the indoor EXV openings increased, as inferred from the decreasing pressure drop through indoor EXV shown in Fig.3(c). This further resulted in a larger refrigerant mass flow rate and thereby smaller suction superheat. As a result, outdoor EXV openings continued to decrease. In this way, the two control loops interfered with each other, so that the EXV openings could not reach a stable state under the steady operating condition.

The above-described phenomenon would cause frequent changes in EXV openings and shorten the devices' service lives. When multiple indoor units are operating, this problem is even more complex because it requires to satisfy different heating loads on multiple indoor units.

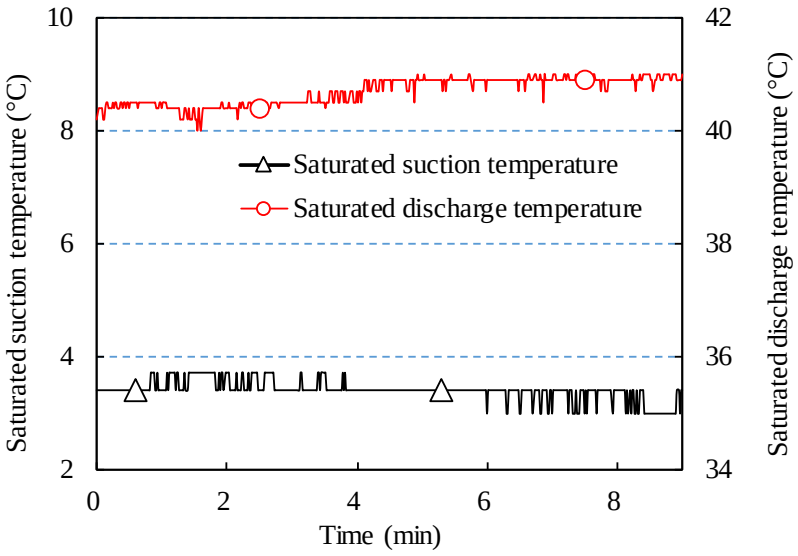


(a) Saturated suction and discharge temperature

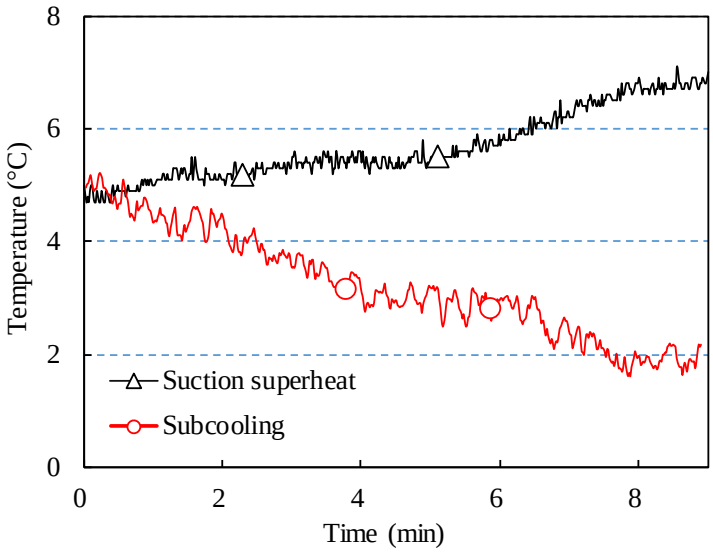


(b) Suction superheat and subcooling

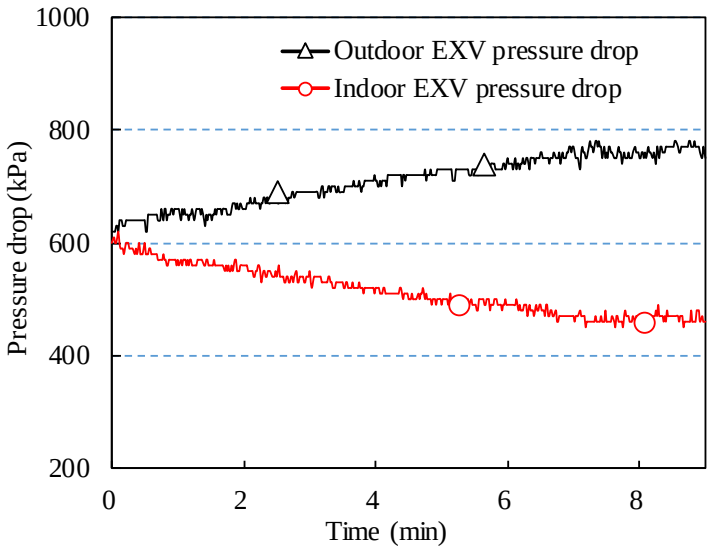


(c) Pressure drop of EXVs

Fig.3 Experimental results of case 1

## 2.2 Case 2

To address the instability of EXV openings, we tried to limit the opening range of the indoor EXVs. For example, we limited the opening to 90–260 pulses (relative to a full opening of 480 pulses) to limit the pressure drop of the indoor EXVs so that a sufficient pressure difference would be retained for the outdoor EXV to control suction superheat. This strategy has been applied to a high-temperature multi-split heat pump system that produces 50–70°C supply air for the drying process of a lithium battery-coating machine. The system consisted of one evaporator and six condensing units, with rated heating capacity of 50 kW and R134a as the refrigerant.

Fig.4 depicts the dynamic response of EXV openings and supply air temperature during the system start-up phase. As shown in Fig.4(a), the indoor and outdoor EXV openings rapidly stabilized. This result suggests that this constrained EXV control strategy could effectively address the instability of EXV openings. However, Fig.4(b) reveals that the supply air temperature could not meet the required set-point due to EXV opening saturation. Specifically, when the supply air temperature set-point of indoor unit 1 is increased and that of indoor unit 2 is kept constant, the supply air temperature of both indoor units will actually increase.

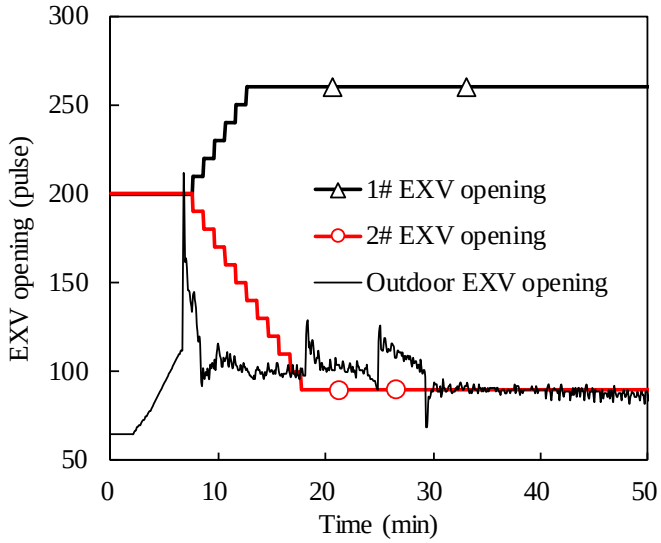


(a) EXV opening

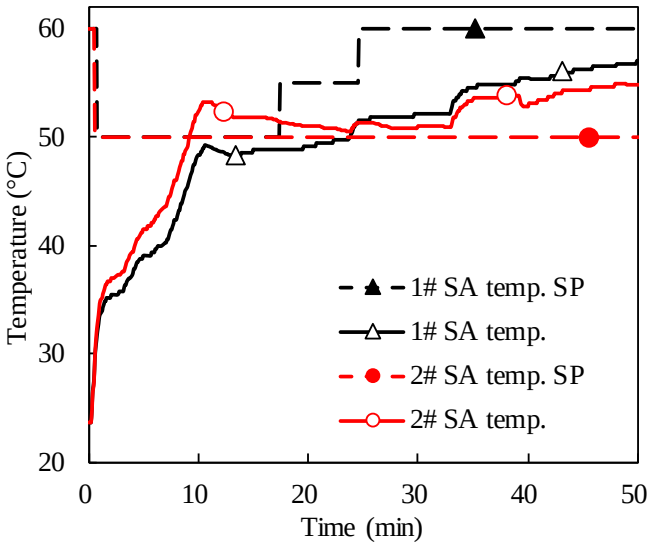


(b) Supply air temperature

Fig.4 Experimental results of case 2

### 2.3 Results analysis

The two experimental cases indicate that the conventional heating control strategy will result in unstable control of the EXV openings, namely EXVs could not reach stable openings under steady operating conditions. In the meantime, the control targets for the supply air temperature, subcooling, and suction superheat are also difficult to meet. Fundamentally, the poor control performance is caused by the defective control structure.

For qualitative analysis, the multi-condenser heat pump can be simplified as a single-condenser heat pump with two EXVs if multiple indoor units share the same heat exchanger area, air inlet, and outlet states, where no refrigerant distribution issue requires consideration. In this case, the conventional heating control strategy works in the same way, with the two EXVs controlling refrigerant subcooling and suction superheat, respectively. Now the control strategy can be found unreasonable. On the one hand, the condenser subcooling significantly affects the active charge of the system [26]. The refrigerant charge determined by the subcooling target is probably not consistent with the actual charge. On the other hand, when the two charges are identical, infinite solutions to EXV openings will exist that satisfy the subcooling and suction superheat targets. Specifically, the refrigerant mass flow rates through indoor and outdoor EXVs are given by Eq. (1) and Eq. (2).

$$m_{\mathrm{u}} = A_{\mathrm{u}}\sqrt{\rho\left(p_{\mathrm{c}} - p_{\mathrm{m}}\right)} \tag{1}$$

$$m_{\mathrm{d}} = A_{\mathrm{d}}\sqrt{\rho\left(p_{\mathrm{m}} - p_{\mathrm{e}}\right)} \tag{2}$$

where the refrigerant density entering the EXVs is assumed to be constant; $p_c$, $p_e$, and $p_m$ refer to the condensing pressure, the evaporating pressure, and the intermediate pressure entering the outdoor EXV, respectively; $A_u$ and $A_d$ are the flow area for the indoor and outdoor EXVs, respectively, which are closely related to EXV openings; and we assume that a certain refrigerant mass flow rate, $m$, satisfies the target subcooling and suction superheat. By substituting $m$ into Eq. (1) and assigning an arbitrary $p_m$, flow area for the two EXVs can be obtained according to Eq. (3) and Eq. (4):

$$A_u = \frac{m}{\sqrt{\rho\left(p_c - p_m\right)}} \tag{3}$$

$$A_d = \frac{m}{\sqrt{\rho\left(p_m - p_e\right)}} \tag{4}$$

Taken together, the conventional heating control strategy brings about redundant constraints for refrigerant charge and under-constraints for EXV openings and intermediate pressure. With the above findings bearing in mind, the conventional heating control strategy applied in multi-condenser systems, in which multiple indoor units are of different sizes and work under different conditions, will face the same dilemma. The refrigerant charge determined by the subcooling targets of indoor units for flow distribution is probably not consistent with the actual charge. When the two charges are identical, infinite solutions to indoor EXVs and outdoor EXV openings exist.

The above analysis has given a qualitative explanation to the specific uncontrollable problem based on system operation characteristics. It is valuable to provide a quantitative and general method to detect similar uncontrollable problems. The following parts will introduce and apply such a method, i.e. functional controllability analysis, to the uncontrollable problem of multi-condenser heat pumps.

# 3 Functional controllability analysis of conventional control strategy

In this section, the concept of functional controllability is first introduced to provide a theoretical insight into the above-mentioned uncontrollability problem. To facilitate functional controllability analysis, a physics-based dynamic model was developed and validated for a two-condenser heat pump system. Functional controllability analysis of the conventional control strategy was then conducted based on the dynamic model.

## 3.1 Introduction to functional controllability

Functional controllability is one of the basic requirements for a control structure. It implies independent control of all outputs with available inputs. This definition was introduced by Rosenbrock [27] for square systems. A plant is functionally uncontrollable if and only if the minimum singular value at any frequency equals zero. Here note that singular values of multi-input multi-output system are computed by performing singular value decomposition of the matrix G(s) at each frequency *s*. For an *m*-input *l*-output system $\mathbf{G}(s) = \mathbf{C}\ (s\mathbf{I} - \mathbf{A})^{-1}\mathbf{B}$, we have that $\mathbf{G}(s)$ is functionally uncontrollable if rank ($\mathbf{B}$) < *l* (the system is input deficient), or if rank($\mathbf{C}$) < *l* (the system is output deficient), or if rank ($s\mathbf{I} - \mathbf{A}$) < *l* (the system has fewer states than outputs) [16].

To numerically analyze the functional controllability of a system, its dynamic model is required to calculate singular values at any frequency. Therefore, a dynamic model of a two-condenser heat pump system is developed. Moreover, for functional controllability analysis, the dynamic model is linearized around a nominal solution into a state-space form and is validated with experiments.

## 3.2 Dynamic modeling

### 3.2.1 Heat exchangers

The moving-boundary method, which can preferentially balance the simulation accuracy and calculating complexity in heat exchanger modeling, has been widely accepted in control-related research. In this study, we use this method for dynamic modeling of evaporator and condenser as well. Assumptions taken in the model are the same as [28]. Evaporator modeling is detailed as follows.

The evaporator can be divided into a two-phase region and a superheated region. Refrigerant mass and energy conservation equations of two-phase region can be expressed as below. The superscript dot in the below equations represent the first derivative of the marked parameters with respect to time.

$$\left(\rho_{\mathrm{le}}-\rho_{\mathrm{ge}}\right)\left(1-\overline{\gamma}_{\mathrm{e}}\right)A_{\mathrm{e}}\dot{L}_{\mathrm{e1}}+\left(\frac{\mathrm{d}\rho_{\mathrm{le}}}{\mathrm{d}p_{\mathrm{e}}}\left(1-\overline{\gamma}_{\mathrm{e}}\right)+\frac{\mathrm{d}\rho_{\mathrm{ge}}}{\mathrm{d}p_{\mathrm{e}}}\overline{\gamma}_{\mathrm{e}}\right)A_{\mathrm{e}}L_{\mathrm{e1}}\dot{p}_{\mathrm{e}}=m_{\mathrm{ei}}-m_{\mathrm{eint}} \tag{5}$$

$$\begin{aligned}&\left(\rho_{\mathrm{le}}h_{\mathrm{le}}-\rho_{\mathrm{ge}}h_{\mathrm{ge}}\right)\left(1-\overline{\gamma}_{\mathrm{e}}\right)A_{\mathrm{e}}\dot{L}_{\mathrm{e1}}+\left(\frac{\mathrm{d}\rho_{\mathrm{le}}h_{\mathrm{le}}}{\mathrm{d}p_{\mathrm{e}}}\left(1-\overline{\gamma}_{\mathrm{e}}\right)+\frac{\mathrm{d}\rho_{\mathrm{ge}}h_{\mathrm{ge}}}{\mathrm{d}p_{\mathrm{e}}}\overline{\gamma}_{\mathrm{e}}-1\right)A_{\mathrm{e}}L_{\mathrm{e1}}\dot{p}_{\mathrm{e}}\\&=m_{\mathrm{ei}}h_{\mathrm{ei}}-m_{\mathrm{eint}}h_{\mathrm{ge}}+\alpha_{\mathrm{e1}}\pi D_{\mathrm{e}}L_{\mathrm{e1}}\left(T_{\mathrm{ew1}}-T_{\mathrm{e}}\right)\end{aligned} \tag{6}$$

Refrigerant energy conservation equation of superheated region is

$$\begin{aligned}&\rho_{\mathrm{ge}}\frac{h_{\mathrm{ge}}-h_{\mathrm{s}}}{2}A_{\mathrm{e}}\dot{L}_{\mathrm{e1}}+\left(\frac{\rho_{\mathrm{ge}}}{2}\left(\frac{\mathrm{d}h_{\mathrm{ge}}}{\mathrm{d}p_{\mathrm{e}}}+\frac{\partial h_{\mathrm{s}}}{\partial p_{\mathrm{e}}}\right)-1\right)A_{\mathrm{e}}L_{\mathrm{e2}}\dot{p}_{\mathrm{e}}+\frac{\rho_{\mathrm{ge}}}{2}\frac{\partial h_{\mathrm{s}}}{\partial T_{\mathrm{s}}}A_{\mathrm{e}}L_{\mathrm{e2}}\dot{T}_{\mathrm{s}}\\&=m_{\mathrm{eint}}\left(h_{\mathrm{ge}}-h_{\mathrm{s}}\right)+\alpha_{\mathrm{e2}}\pi D_{\mathrm{e}}L_{\mathrm{e2}}\left(T_{\mathrm{ew2}}-\left(T_{\mathrm{e}}+T_{\mathrm{s}}\right)/2\right)\end{aligned}\tag{7}$$

Energy equation for the tube wall of two-phase region is based on the weighted mean wall temperature [29].

$$\begin{aligned}&\rho_{\mathrm{w}}c_{\mathrm{w}}A_{\mathrm{w}}\frac{L_{\mathrm{e1}}}{L_{\mathrm{e}}}\left(T_{\mathrm{ew1}}-T_{\mathrm{ew2}}\right)\dot{L}_{\mathrm{e1}}+\rho_{\mathrm{w}}c_{\mathrm{w}}A_{\mathrm{w}}L_{\mathrm{e1}}\dot{T}_{\mathrm{ew1}}\\&=\alpha_{\mathrm{e1}}\pi D_{\mathrm{e}}L_{\mathrm{e1}}\left(T_{\mathrm{e}}-T_{\mathrm{ew1}}\right)+\alpha_{\mathrm{eo}}\pi D_{\mathrm{e}}L_{\mathrm{e1}}\left(T_{\mathrm{ea1}}-T_{\mathrm{ew1}}\right)/A_{\mathrm{r}}\end{aligned}\tag{8}$$

Energy equation for the tube wall of superheated region is

$$\begin{aligned}&\rho_{\mathrm{w}}c_{\mathrm{w}}A_{\mathrm{w}}\frac{L_{\mathrm{e2}}}{L_{\mathrm{e}}}\left(T_{\mathrm{ew1}}-T_{\mathrm{ew2}}\right)\dot{L}_{\mathrm{e1}}+\rho_{\mathrm{w}}c_{\mathrm{w}}A_{\mathrm{w}}L_{\mathrm{e2}}\dot{T}_{\mathrm{ew2}}\\&=\alpha_{\mathrm{e2}}\pi D_{\mathrm{e}}L_{\mathrm{e2}}\left[\left(T_{\mathrm{e}}+T_{\mathrm{s}}\right)/2-T_{\mathrm{ew2}}\right]+\alpha_{\mathrm{eo}}\pi D_{\mathrm{e}}L_{\mathrm{e2}}\left(T_{\mathrm{ea2}}-T_{\mathrm{ew2}}\right)/A_{\mathrm{r}}\end{aligned}\tag{9}$$

Equations (5) through (9) are five governing equations describing dynamics of an evaporator, which can be written in a compact state space form.

$$\mathbf{F}_{\mathrm{e}}\dot{\mathbf{X}}_{\mathrm{e}}=G\left(\mathbf{X}_{\mathrm{e}},\mathbf{Y}_{\mathrm{e}}\right)\tag{10}$$

Likewise, condenser model details can be found in Appendix A.1.

### 3.2.2 Compressor

The dynamics of refrigerant mass flow rate through a compressor are much faster than that of the heat exchangers. Therefore, a steady-state polynomial equation [30] is selected to predict the variable-speed compressor performance, as shown in Eq. (11).

$$\begin{aligned}y_{\mathrm{comp}}&=c_1+c_2T_{\mathrm{e}}+c_3T_{\mathrm{c}}+c_4f_{\mathrm{r}}+c_5T_{\mathrm{e}}^2+c_6T_{\mathrm{c}}^2+c_7f_{\mathrm{r}}^2+c_8T_{\mathrm{e}}T_{\mathrm{c}}+c_9T_{\mathrm{e}}f_{\mathrm{r}}+c_{10}T_{\mathrm{c}}f_{\mathrm{r}}\\&+c_{11}T_{\mathrm{e}}^2f_{\mathrm{r}}+c_{12}T_{\mathrm{e}}f_{\mathrm{r}}^2+c_{13}T_{\mathrm{c}}^2f_{\mathrm{r}}+c_{14}T_{\mathrm{c}}f_{\mathrm{r}}^2+c_{15}T_{\mathrm{e}}T_{\mathrm{c}}f_{\mathrm{r}}\end{aligned}\tag{11}$$

where $y$ stands for the refrigerant mass flow rate or power consumption of compressor and $T_{\mathrm{c}}$, $T_{\mathrm{e}}$, $f_{\mathrm{r}}$ represent the condensing temperature, evaporating temperature, and compressor frequency, respectively. Coefficients $c_1$ to $c_{15}$ are curve-fitted using the data supplied by the compressor manufacturer.

Considering the relatively large thermal capacity of a compressor, a lumped parameter thermal model was developed in which the temperatures of the shell, motor, lubricating oil and discharged refrigerant are assumed to be the same. This assumption is acceptable for hot shell compressors. Heat transfer between the compressor and the external environment involves both convection and radiation. The energy balance equation of the compressor is given by Eq. (12).

$$M_{\mathrm{comp}} c_{\mathrm{comp}} \dot{T}_{\mathrm{d}} = m_{\mathrm{comp}} \left(h_{\mathrm{s}} - h_{\mathrm{d}}\right) + W_{\mathrm{comp}} - \alpha_{\mathrm{comp}} A_{\mathrm{comp}} \left(T_{\mathrm{d}} - T_{\mathrm{amb}}\right) - \varepsilon\sigma A_{\mathrm{comp}} \left(T_{\mathrm{d}}^{4} - T_{\mathrm{amb}}^{4}\right) \tag{12}$$

### 3.2.3 Expansion valve

Given that dynamic response of EXV is also much faster than that of heat exchangers, steady-state EXV model is used.

$$m_{\mathrm{exv}} = A_{\mathrm{exv}} \sqrt{\rho\left(p_{\mathrm{c}} - p_{\mathrm{e}}\right)} \tag{13}$$

### 3.2.4 System modeling

When integrating component models into a system model, some additional constraints must be considered, including the refrigerant mass conservation equation of the whole cycle and the refrigerant mass flow distribution among multiple indoor units.

The refrigerant system is a closed cycle and hence the total refrigerant charge conservation equation stands. Taking the two-condenser heat pump system depicted in Fig.1 as an example, its total refrigerant mass equation is given by Eq. (14).

$$m_{\mathrm{ei}} - m_{\mathrm{eo}} + m_{\mathrm{ci},1} - m_{\mathrm{co},1} + m_{\mathrm{ci},2} - m_{\mathrm{co},2} = 0 \tag{14}$$

By substituting in the mass equation of each component, we can obtain Eq. (15).

$$\begin{aligned}
&\left(\rho_{\mathrm{le}} - \rho_{\mathrm{ge}}\right)\left(1-\overline{\gamma}_{\mathrm{e}}\right) A_{\mathrm{e}} \dot{L}_{\mathrm{e1}} + \left(\frac{\mathrm{d}\rho_{\mathrm{le}}}{\mathrm{d}p_{\mathrm{e}}}\left(1-\overline{\gamma}_{\mathrm{e}}\right) + \frac{\mathrm{d}\rho_{\mathrm{ge}}}{\mathrm{d}p_{\mathrm{e}}}\overline{\gamma}_{\mathrm{e}}\right) A_{\mathrm{e}} L_{\mathrm{e1}} \dot{p}_{\mathrm{e}} \\
&+\left(\rho_{\mathrm{gc}} - \rho_{\mathrm{lc}}\right) A_{\mathrm{c}} \dot{L}_{\mathrm{c1\text{-}1}} + \left(\rho_{\mathrm{gc}} - \rho_{\mathrm{lc}}\right)\overline{\gamma}_{\mathrm{c}} A_{\mathrm{c}} \dot{L}_{\mathrm{c2\text{-}1}} + \left(\frac{\mathrm{d}\rho_{\mathrm{lc}}}{\mathrm{d}p_{\mathrm{c}}}\left(1-\overline{\gamma}_{\mathrm{c}}\right) + \frac{\mathrm{d}\rho_{\mathrm{gc}}}{\mathrm{d}p_{\mathrm{c}}}\overline{\gamma}_{\mathrm{c}}\right) A_{\mathrm{c}} L_{\mathrm{c2\text{-}1}} \dot{p}_{\mathrm{c1}} \\
&+\left(\rho_{\mathrm{gc}} - \rho_{\mathrm{lc}}\right) A_{\mathrm{c}} \dot{L}_{\mathrm{c1\text{-}2}} + \left(\rho_{\mathrm{gc}} - \rho_{\mathrm{lc}}\right)\overline{\gamma}_{\mathrm{c}} A_{\mathrm{c}} \dot{L}_{\mathrm{c2\text{-}2}} + \left(\frac{\mathrm{d}\rho_{\mathrm{lc}}}{\mathrm{d}p_{\mathrm{c}}}\left(1-\overline{\gamma}_{\mathrm{c}}\right) + \frac{\mathrm{d}\rho_{\mathrm{gc}}}{\mathrm{d}p_{\mathrm{c}}}\overline{\gamma}_{\mathrm{c}}\right) A_{\mathrm{c}} L_{\mathrm{c2\text{-}2}} \dot{p}_{\mathrm{c2}} = 0
\end{aligned} \tag{15}$$

According to Eq. (15), $p_{\mathrm{e}}$ could be expressed as a function of $L_{\mathrm{e1}}$, $L_{\mathrm{c1\text{-}1}}$, $L_{\mathrm{c2\text{-}1}}$, $p_{\mathrm{c1}}$, $L_{\mathrm{c1\text{-}2}}$, $L_{\mathrm{c2\text{-}2}}$, and $p_{\mathrm{c2}}$. Therefore, when integrating component models into a system model, the number of state variables of the system equals that of the components minus 1, so that the system model does not include redundant state variables.

Refrigerant mass flow distribution among multiple indoor units is determined by the pressure drop of each indoor branch. The calculation of the refrigerant pressure drop is basically related to the momentum equation. Zhang et al. [31] found that the results with transient and steady-state momentum equations are pretty close, wherein the latter is more robust and faster in computation. Consequently, a steady-state pressure drop equation given by Eq. (16) is adopted, where the coefficient $K$ is curve-fitted using experimental results.

$$\Delta p = Km^2 \tag{16}$$

Then, refrigerant mass flow rate entering the two condensers, $m_{ci1}$ and $m_{ci2}$, can be obtained by Eq. (17).

$$\begin{cases} m_{ci,1} = \sqrt{\dfrac{p_c - p_{c1}}{K}} \\ m_{ci,2} = \sqrt{\dfrac{p_c - p_{c2}}{K}} \\ \\ m_{ci,1} + m_{ci,2} = m_{comp} \end{cases} \tag{17}$$

where $p_c$, $p_{c1}$, and $p_{c2}$ represent compressor discharge pressure and condensing pressure of the two indoor units, respectively.

3.2.5 Model linearization

Taking the constraints for refrigerant charge and refrigerant flow distribution into consideration, the system model can be formed by integrating component models together, as given by Eq. (18).

$$\mathbf{F}\dot{\mathbf{X}} = G(\mathbf{X}, \mathbf{U}) \tag{18}$$

The right side of Eq. (18), $G$ ($\mathbf{X}$, $\mathbf{U}$), is nonlinear expressions of state variables and input variables, as detailed in Appendix A.2. To simplify Eq. (18) into a linear state space form, the system model is linearized around a nominal solution. Deviation variables $\delta\mathbf{X}$ and $\delta\mathbf{U}$ are introduced to describe system dynamics in the vicinity of a predetermined equilibrium point [28, 32], as per Eq. (19).

$$\begin{cases} \mathbf{X} = \mathbf{X}^s + \delta\mathbf{X}, \\ \mathbf{U} = \mathbf{U}^s + \delta\mathbf{U}, \\ \delta G = \left.\dfrac{\partial G}{\partial \mathbf{X}}\right|_{\mathbf{X}^s} \delta\mathbf{X} + \left.\dfrac{\partial G}{\partial \mathbf{U}}\right|_{\mathbf{U}^s} \delta\mathbf{U} \end{cases} \tag{19}$$

Thereby the nonlinear $G$ ($\mathbf{X}$, $\mathbf{U}$) can be simplified as Eq. (20).

$$G(\mathbf{X}, \mathbf{U}) = \mathbf{M}\mathbf{X} + \mathbf{N}\mathbf{U} \tag{20}$$

Finally, the linear system model for the two-condenser heat pump system is established

$$\begin{cases} \dot{\mathbf{X}} = \mathbf{A}\mathbf{X} + \mathbf{B}\mathbf{U}, \mathbf{A} = \mathbf{F}^{-1}\mathbf{M}, \ \mathbf{B} = \mathbf{F}^{-1}\mathbf{N} \\ \mathbf{Y} = \mathbf{C}\mathbf{X} + \mathbf{D}\mathbf{U} \end{cases} \tag{21}$$

where input variables $\mathbf{U} = [f, A_1, A_2, A_d]$, output variables $\mathbf{Y} = [T_c, T_{ca\_out\text{-}1}, T_{ca\_out\text{-}2}, T_{sh}]$.

### 3.3 Model validation

To validate the dynamic model developed in Section 3.2, simulation results were compared with experimental data. Fig.5(a) and Fig.5(b) depict the open loop dynamic response to a step increase in compressor speed, where Fig.5(a) compares the simulated suction superheat and evaporating temperature, and Fig.5(b) compares discharge superheat and condensing temperature. Fig.5(c) and Fig.5(d) depict the open loop dynamic response to a step increase in outdoor EXV opening. As observed, simulations tracked the actual dynamic response of key operating parameters reasonably well. Thus, although the linear state-space model is much simplified from the actual nonlinear system, it could reasonably replicate main dynamics of the system.

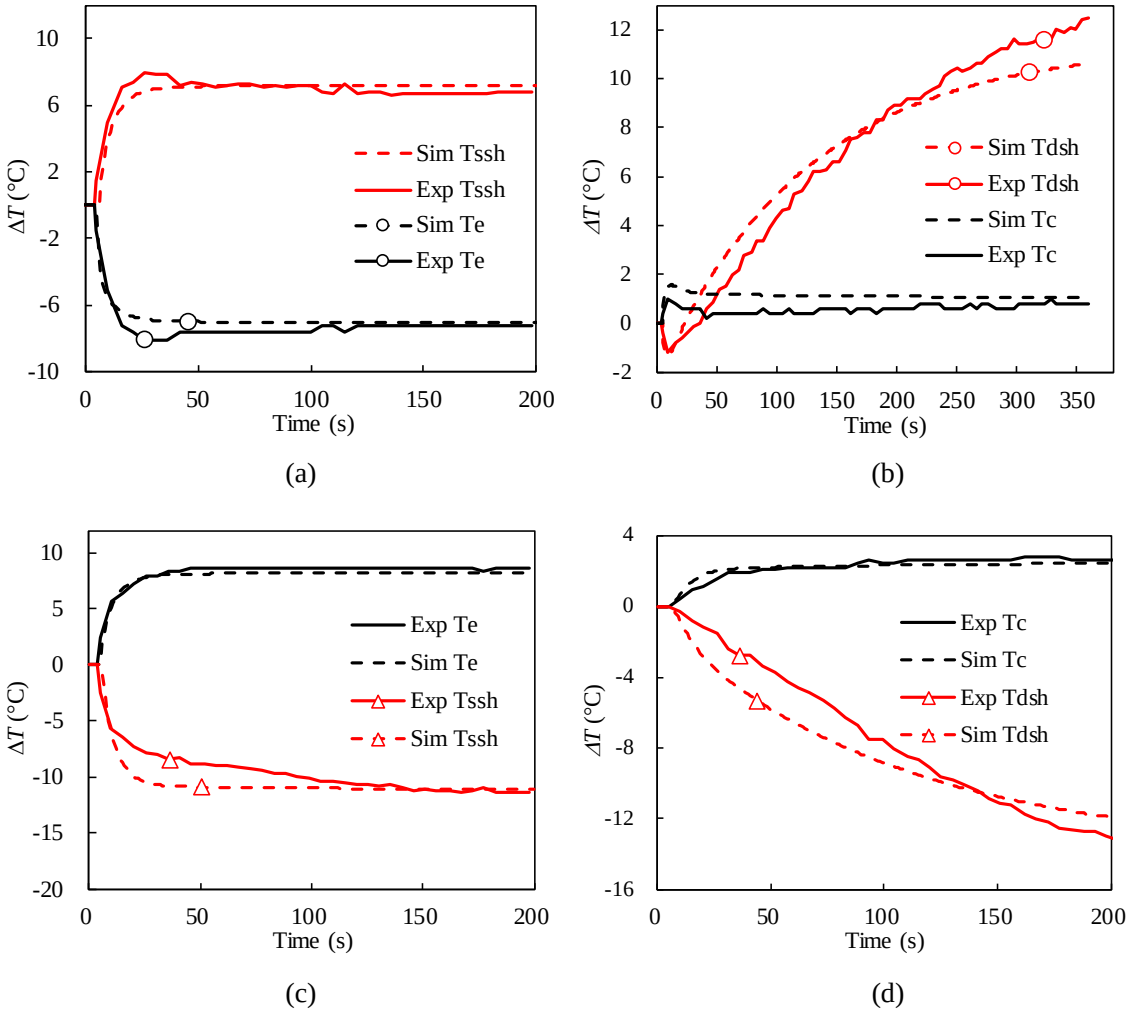


(Sim – simulated; Exp – experimental; Tssh – suction superheat; Te – evaporating temperature; Tdsh – discharge superheat; Tc – condensing temperature)

Fig.5 Dynamic response to a step-increase in compressor speed and outdoor EXV opening

### 3.4 Functional controllability analysis

As mentioned in Section 3.1, a plant is functionally uncontrollable if and only if the minimum singular value at any frequency equals zero. Singular values of the two-condenser heat pump system are numerically calculated using Control System Toolbox in MATLAB, as shown in Fig.6. According to theorems from linear algebra, there exists *m* different singular values for an *m* by *m* matrix. The four curves in Fig.6 represent four singular values of the four-input four-output heat pump system model varying with frequency. The results indicate that the minimum singular value is less than -300 dB ($10^{-15}$). Considering the computational accuracy, we could assume that the minimum singular value at any frequency equals zero. Consequently, the conventional heating control strategy-based heat pump system is functionally uncontrollable.

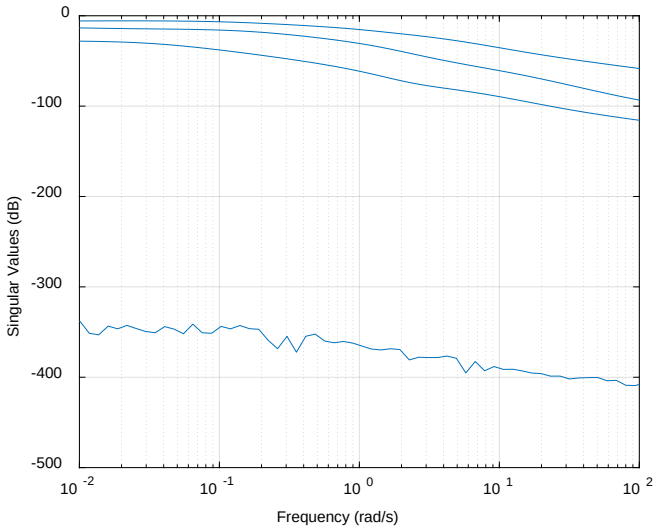


Fig.6 Singular values of the two-condenser heat pump system

What follows will prove in theory that matrix **B** in the state space model of the two-condenser heat pump system is singular, i.e., rank (**B**) < *l*. Thereby the system $\mathbf{G}(s) = \mathbf{C}(s\mathbf{I} - \mathbf{A})^{-1}\mathbf{B}$ is input deficient, which implies functional uncontrollability.

The numerical results show that the fourth column in matrix **B** and **N** is a linear combination of the second and third column (Note that $\mathbf{B} = \mathbf{F}^{-1}\mathbf{N}$). To theoretically prove linear dependence among the three columns, we first assume a linear combination coefficient $\varepsilon$. If the linear dependence holds, the combined ratio of different rows given by Eq. (22) equals to each

other.

$$\begin{cases} \dfrac{N(1,2)+\varepsilon N(1,3)}{N(1,4)} = \left(\dfrac{\partial m_{\mathrm{d}}}{\partial A_1}+\varepsilon\dfrac{\partial m_{\mathrm{d}}}{\partial A_2}\right)\Big/\dfrac{\partial m_{\mathrm{d}}}{\partial A_{\mathrm{d}}}, \\ \dfrac{N(6,2)+\varepsilon N(6,3)}{N(6,4)} = \dfrac{N(8,2)+\varepsilon N(8,3)}{N(8,4)} = \dfrac{N(9,2)+\varepsilon N(9,3)}{N(9,4)} \\ \qquad = \left(\dfrac{\partial m_{\text{co-1}}}{\partial A_1}+\varepsilon\dfrac{\partial m_{\text{co-1}}}{\partial A_2}\right)\Big/\dfrac{\partial m_{\text{co-1}}}{\partial A_{\mathrm{d}}}, \\ \dfrac{N(13,2)+\varepsilon N(13,3)}{N(13,4)} = \dfrac{N(15,2)+\varepsilon N(15,3)}{N(15,4)} = \dfrac{N(16,2)+\varepsilon N(16,3)}{N(16,4)} \\ \qquad = \left(\dfrac{\partial m_{\text{co-2}}}{\partial A_1}+\varepsilon\dfrac{\partial m_{\text{co-2}}}{\partial A_2}\right)\Big/\dfrac{\partial m_{\text{co-2}}}{\partial A_{\mathrm{d}}} \end{cases} \tag{22}$$

In other words, we should prove Eq. (23).

$$\left(\frac{\partial m_{\mathrm{d}}}{\partial A_1}+\varepsilon\frac{\partial m_{\mathrm{d}}}{\partial A_2}\right)\Big/\frac{\partial m_{\mathrm{d}}}{\partial A_{\mathrm{d}}} = \left(\frac{\partial m_{\text{co-1}}}{\partial A_1}+\varepsilon\frac{\partial m_{\text{co-1}}}{\partial A_2}\right)\Big/\frac{\partial m_{\text{co-1}}}{\partial A_{\mathrm{d}}} = \left(\frac{\partial m_{\text{co-2}}}{\partial A_1}+\varepsilon\frac{\partial m_{\text{co-2}}}{\partial A_2}\right)\Big/\frac{\partial m_{\text{co-2}}}{\partial A_{\mathrm{d}}} \tag{23}$$

To reach Eq. (23), first derivatives of $m_{\mathrm{d}}$, $m_{\text{co-1}}$ and $m_{\text{co-2}}$ with respect to $A_{\mathrm{d}}$, $A_1$, $A_2$ are obtained by taking the derivatives of mass flow rate (Eq. (24)) subject to the constraints of equal refrigerant mass flow rate through the indoor EXVs and outdoor EXV (Eq. (25)).

$$\begin{aligned} \delta m_{\mathrm{d}} &= \delta\left(A_{\mathrm{d}}\sqrt{\rho_{\mathrm{lm}}\left(p_{\mathrm{m}}-p_{\mathrm{e}}\right)}\right) \\ &= -\frac{A_{\mathrm{d}}\rho_{\mathrm{lm}}}{2\sqrt{\rho_{\mathrm{lm}}\left(p_{\mathrm{m}}-p_{\mathrm{e}}\right)}}\delta p_{\mathrm{e}} + \frac{A_{\mathrm{d}}\rho_{\mathrm{lm}}}{2\sqrt{\rho_{\mathrm{lm}}\left(p_{\mathrm{m}}-p_{\mathrm{e}}\right)}}\delta p_{\mathrm{m}} + \sqrt{\rho_{\mathrm{lm}}\left(p_{\mathrm{m}}-p_{\mathrm{e}}\right)}\delta A_{\mathrm{d}} \\ &= k_{\text{d-exv,1}}\delta p_{\mathrm{e}} + k_{\text{d-exv,2}}\delta p_{\mathrm{m}} + k_{\text{d-exv,3}}\delta A_{\mathrm{d}} \end{aligned} \tag{24}$$

where $k$ represents first derivatives of its subscript variable with respect to the state variables and input variables.

$$A_1\sqrt{\rho_{\text{liq-1}}\left(p_{\mathrm{c1}}-p_{\mathrm{m}}\right)} + A_2\sqrt{\rho_{\text{liq-2}}\left(p_{\mathrm{c2}}-p_{\mathrm{m}}\right)} = A_{\mathrm{d}}\sqrt{\rho_{\mathrm{lm}}\left(p_{\mathrm{m}}-p_{\mathrm{e}}\right)} \tag{25}$$

Then the partial derivatives of $m_{\mathrm{d}}$ with respect to $A_{\mathrm{d}}$, $A_1$, $A_2$ are

$$\begin{cases} \dfrac{\partial m_{\mathrm{d}}}{\partial A_1} = -\dfrac{k_{\mathrm{d-exv,2}}k_{\text{u-exv1,3}}}{k_{\text{u-exv1,1}}+k_{\text{u-exv2,1}}-k_{\text{d-exv,2}}} \\ \dfrac{\partial m_{\mathrm{d}}}{\partial A_2} = -\dfrac{k_{\mathrm{d-exv,2}}k_{\text{u-exv2,3}}}{k_{\text{u-exv1,1}}+k_{\text{u-exv2,1}}-k_{\text{d-exv,2}}} \\ \dfrac{\partial m_{\mathrm{d}}}{\partial A_{\mathrm{d}}} = \dfrac{k_{\mathrm{d-exv,2}}k_{\text{d-exv,3}}}{k_{\text{u-exv1,1}}+k_{\text{u-exv2,1}}-k_{\text{d-exv,2}}} + k_{\mathrm{d-exv,3}} \end{cases} \tag{26}$$

The first term in Eq. (23) is simplified as

$$\left(\frac{\partial m_{\mathrm{d}}}{\partial A_1}+\varepsilon\frac{\partial m_{\mathrm{d}}}{\partial A_2}\right)\Big/\frac{\partial m_{\mathrm{d}}}{\partial A_{\mathrm{d}}}=-\frac{k_{\mathrm{d-exv},2}k_{\mathrm{u\text{-}exv1,3}}+\varepsilon k_{\mathrm{d-exv},2}k_{\mathrm{u\text{-}exv2,3}}}{k_{\mathrm{d\text{-}exv,3}}\left(k_{\mathrm{u\text{-}exv1,1}}+k_{\mathrm{u\text{-}exv2,1}}\right)} \tag{27}$$

Likewise, we have

$$\left(\frac{\partial m_{\mathrm{co-1}}}{\partial A_1}+\varepsilon\frac{\partial m_{\mathrm{co-1}}}{\partial A_2}\right)\Big/\frac{\partial m_{\mathrm{co\text{-}1}}}{\partial A_{\mathrm{d}}}=\frac{k_{\mathrm{u-exv1,3}}k_{\mathrm{u\text{-}exv2,1}}-k_{\mathrm{u\text{-}exv1,3}}k_{\mathrm{d-exv,2}}-\varepsilon k_{\mathrm{u-exv1,1}}k_{\mathrm{u\text{-}exv2,3}}}{k_{\mathrm{u-exv1,1}}k_{\mathrm{d\text{-}exv,3}}} \tag{28}$$

$$\left(\frac{\partial m_{\mathrm{co-2}}}{\partial A_1}+\varepsilon\frac{\partial m_{\mathrm{co-2}}}{\partial A_2}\right)\Big/\frac{\partial m_{\mathrm{co\text{-}2}}}{\partial A_{\mathrm{d}}}=\frac{\varepsilon k_{\mathrm{u-exv2,3}}k_{\mathrm{u\text{-}exv1,1}}-\varepsilon k_{\mathrm{u-exv2,3}}k_{\mathrm{d\text{-}exv,2}}-k_{\mathrm{u-exv2,1}}k_{\mathrm{u\text{-}exv1,3}}}{k_{\mathrm{u-exv2,1}}k_{\mathrm{d\text{-}exv,3}}} \tag{29}$$

The linear combination coefficient $\varepsilon$ is obtained by setting Eq. (28) equal to Eq. (29), as per Eq. (30).

$$\varepsilon=\frac{k_{\mathrm{u-exv1,3}}k_{\mathrm{u\text{-}exv2,1}}}{k_{\mathrm{u-exv2,3}}k_{\mathrm{u\text{-}exv1,1}}} \tag{30}$$

Then, by substitution of Eq. (30) back into Eq. (28) and Eq. (27), we can obtain

$$\left(\frac{\partial m_{\mathrm{co-1}}}{\partial A_1}+\varepsilon\frac{\partial m_{\mathrm{co-1}}}{\partial A_2}\right)\Big/\frac{\partial m_{\mathrm{co\text{-}1}}}{\partial A_{\mathrm{d}}}=\left(\frac{\partial m_{\mathrm{d-exv}}}{\partial A_1}+\varepsilon\frac{\partial m_{\mathrm{d-exv}}}{\partial A_2}\right)\Big/\frac{\partial m_{\mathrm{d-exv}}}{\partial A_{\mathrm{d}}}=-\frac{k_{\mathrm{u\text{-}exv1,3}}k_{\mathrm{d-exv,2}}}{k_{\mathrm{u\text{-}exv1,1}}k_{\mathrm{d\text{-}exv,3}}} \tag{31}$$

Hence Eq. (23) holds, namely matrix **N** and **B** are singular. The two-condenser heat pump system based on conventional control strategy has thus been proven functionally uncontrollable.

The above matrix-based analysis could also enable a theoretical explanation of the problem of redundant constraints for refrigerant charge and under-constraints for EXV openings. The transfer function matrix $\mathbf{G}(s) = \mathbf{C}\,(s\mathbf{I} - \mathbf{A})^{-1}\mathbf{B}$ is singular at any given frequency because of a singular matrix **B**. When $s$ equals zero, $\mathbf{G}(s)$ is actually the system steady-state gain matrix $\mathbf{G}_0$. Here, we consider a linear equation $\mathbf{G}_0\mathbf{U} = \mathbf{Y}$. System control behavior comes down to finding solutions $\mathbf{U} = [f\ A_1\ A_2\ A_{\mathrm{d}}]^{\mathrm{T}}$ to the equation with a given $\mathbf{Y} = [T_{\mathrm{c}}\ T_{\mathrm{ca,out\text{-}1}}\ T_{\mathrm{ca,out\text{-}2}}\ T_{\mathrm{sh}}]^{\mathrm{T}}$. According to theorems from linear algebra, solutions of $\mathbf{Ax} = \mathbf{b}$ exist if and only if Rank (**A**) = Rank (**A** | **b**). Aside from this, the solution is unique with a nonsingular **A**; while there are infinitely many solutions with a singular **A** [33].

Next, we re-examine the multi-condenser heat pump system $\mathbf{G}_0\mathbf{U} = \mathbf{Y}$. Because $\mathbf{G}_0$ is singular, solutions to the equation $\mathbf{G}_0\mathbf{U} = \mathbf{Y}$ exist as infinite solutions only if **Y** is a linear combination of columns from $\mathbf{G}_0$. This conforms to the case in which infinite solutions to EXV openings exist when the real charge agrees with the charge determined by target subcooling. On the other side, if **Y** is not a linear combination of columns from $\mathbf{G}_0$, the equation has no solution. This corresponds to the situation in which the two charges conflict with each other and no possible EXV openings meet the control targets.

# 4 Modified system configuration and control strategy

In this section, a modified system configuration and control strategy is proposed to address the problems caused by the conventional control strategy. Functional controllability analysis of the modified control strategy is conducted. Command-following performance with the two control strategies is compared in simulation tests.

## 4.1 A modified system configuration and control strategy

Functional controllability analysis demonstrates that the heat pump system with conventional heating control strategy is input deficient. The input vector contributed from the outdoor EXV is a linear combination of the output vectors contributed from the indoor EXVs. This is resulted from the deduced intermediate pressure constrained by equal refrigerant mass flow rate through the indoor EXVs and outdoor EXV, as per Eq. (25). One promising solution is to make the intermediate pressure an independent state variable, rather than a deduced variable determined by existing states and inputs variables. It can be achieved by placing a receiver between the indoor EXVs and outdoor EXV. In this way, the intermediate pressure $p_{\mathrm{m}}$ becomes an independent state, like condensing pressure $p_{\mathrm{c1}}$ and $p_{\mathrm{c2}}$. Therefore, a modified system with a receiver located between the indoor EXVs and outdoor EXV is proposed, as shown in Fig.7.

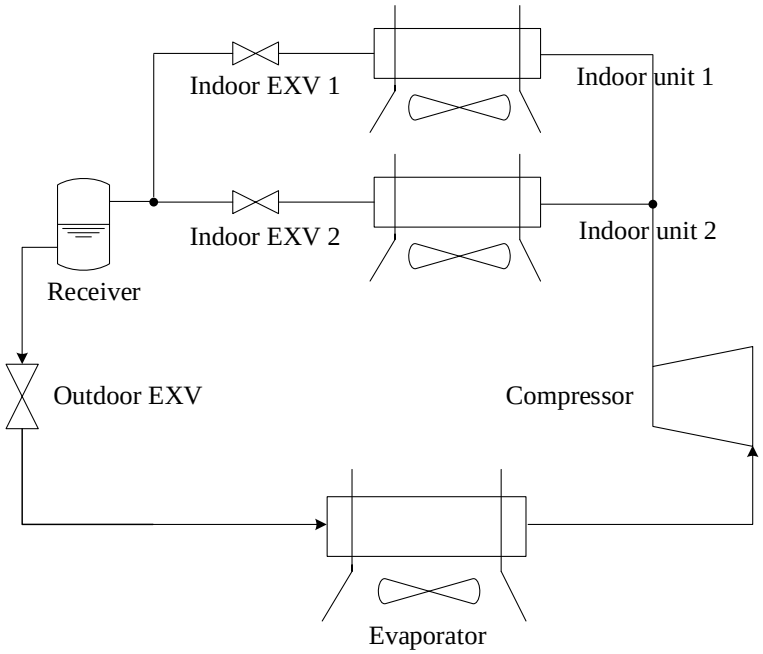


Fig.7 Schematic of a multi-split refrigeration / heat pump system with receiver

From the perceptive of system operation characteristics, the root cause of the

uncontrollable problem with conventional strategy is that we attempted to control subcooling using indoor EXV, which actually equates to controlling the refrigerant charge. The modified system could solve this problem by the use of a receiver. With EXVs control, lower or higher liquid level in the receiver will result in more or less active refrigerant charge in system. By assuming negligible heat leakage from the receiver to the ambient, refrigerant entering and leaving the receiver would be saturated liquid at steady state. Therefore, pressure drop through the indoor EXVs is completely determined by target subcooling. In other words, Eq. (3) has only solution to $A_u$ and $A_d$. Thus, problems of redundant constraints for refrigerant charge and under-constraints for EXV openings have been appropriately solved.

A dynamic model for the modified system is developed with the same approach adopted in Section 3.2. Mass equation of the receiver is given by Eq. (32).

$$A_m\left(\frac{d\rho_{lm}}{dp_m}L_m+\frac{d\rho_{gm}}{dp_m}\left(H-L_m\right)\right)\dot{p}_m=m_{ri}-m_{ro} \tag{32}$$

where $A_m$, $H$ and $L_m$ refer to cross-sectional area, height and liquid level of the receiver, respectively.

Ignoring heat leakage to the ambient air, its energy equation can be written as Eq. (33).

$$A_m\left(\frac{d\rho_{lm}h_{lm}}{dp_m}L_m+\frac{d\rho_{gm}h_{gm}}{dp_m}\left(H-L_m\right)-H\right)\dot{p}_m=m_{ri}h_{ri}-m_{ro}h_{lm} \tag{33}$$

where $p_m$, $\rho_{gm}$, $\rho_{lm}$, $h_{gm}$ and $h_{lm}$ represent pressure, density and specific enthalpy of saturated gas and liquid in the receiver, respectively.

Inputs and outputs of the modified system with a receiver are identical to those of the conventional control strategy, i.e., $\mathbf{U} = [f, A_1, A_2, A_d]$, $\mathbf{Y} = [T_c, T_{ca\_out\text{-}1}, T_{ca\_out\text{-}2}, T_{sh}]$. Singular values of the modified system are numerically calculated, as shown in Fig.8. The four curves represent four singular values of the modified heat pump system varying with frequency. It indicates the minimum singular value is nonzero at any frequency. Therefore, the modified system is functionally controllable.

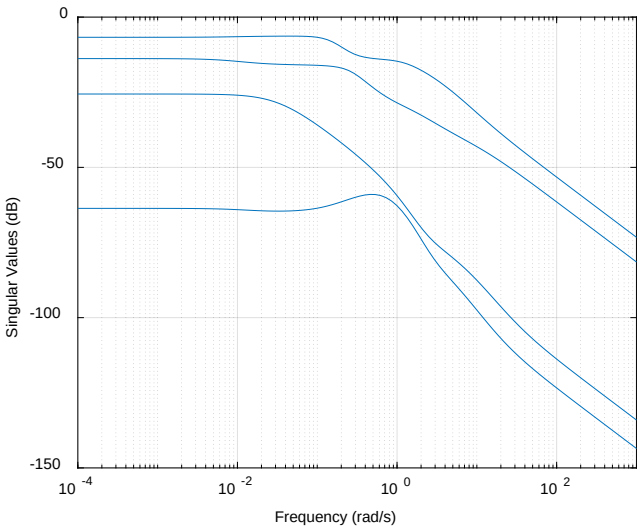


Fig.8 Singular values of the two-condenser heat pump system with a receiver

## 4.2 Control performance comparison

### 4.2.1 Control performance with conventional control strategy

A PI controller was designed and implemented in the validated dynamic model to qualitatively simulate the uncontrollable experimental results. Fig.9(a) presents the command-following performance with the conventional heating control strategy, where control target **Y** = [0 1 0 0] is imposed from time $t$ = 0 s. The control targets represent the desired change in each output relative to the initial state; that is, the supply air temperature of indoor unit 1 ($T_{ca\_out\text{-}1}$) should increase by 1 °C, and supply air temperature for indoor unit 2 ($T_{ca\_out\text{-}2}$), condensing temperature ($T_c$) and suction superheat ($T_{sh}$) must remain constant. Note that inputs and outputs shown in Fig.9 are variations from the original conditions. As can be seen, the controlled variables, except for the condensing temperature, all failed to meet the target settings. As for the inputs, the openings of two indoor EXVs continuously increased, whereas that of the outdoor EXV proportionally and continuously decreased. Simulation results in Fig.9(a) conform with the findings obtained by functional controllability analysis. That is, when **Y** is not a linear combination of columns from $\mathbf{G}_0$, the equation has no solution. The simulations of Fig.9(a) also agree with the experimental results described in Fig.3.

Fig.9(b) shows another set of command-following performance in the system using conventional heating control strategy, where control target **Y** = [1.3429 0.6896 0.6896 -2.1029] and is a linear combination of columns from the steady-state gain matrix $\mathbf{G}_0$. The change of setpoints for the four outputs represented by vector **Y** is introduced from 0 s. A small

disturbance in the reference setting of $T_{ca,out-2}$ is introduced during the 651 – 700 s period. The simulation results demonstrate that the control targets for outputs can be followed perfectly. However, Fig.9(b) indicates that indoor and outdoor EXV stabilize at different openings before and after the disturbance is introduced. Thus the conclusion from the functional controllability analysis is verified. That is, infinite solutions exist to the equation $\mathbf{G}_0\mathbf{U} = \mathbf{Y}$ when $\mathbf{Y}$ is a linear combination of columns from $\mathbf{G}_0$.

In Section 2.2, we attempted to impose constraints on indoor EXV openings to stabilize the system. Fig.9(c) shows the simulation results from the constrained control strategy. The maximum-allowed opening for indoor EXV is set to ± 100 pulses and the control target $\mathbf{Y}$ = [0 1 0 0] is imposed from 0 s. As can be seen from the figure, although both indoor and outdoor EXV reached stable openings, supply air temperatures, $T_{ca\_out-1}$ and $T_{ca\_out-2}$, still failed to meet target settings. Simulations of Fig.9(c) accord with experimental results described in Fig.4.

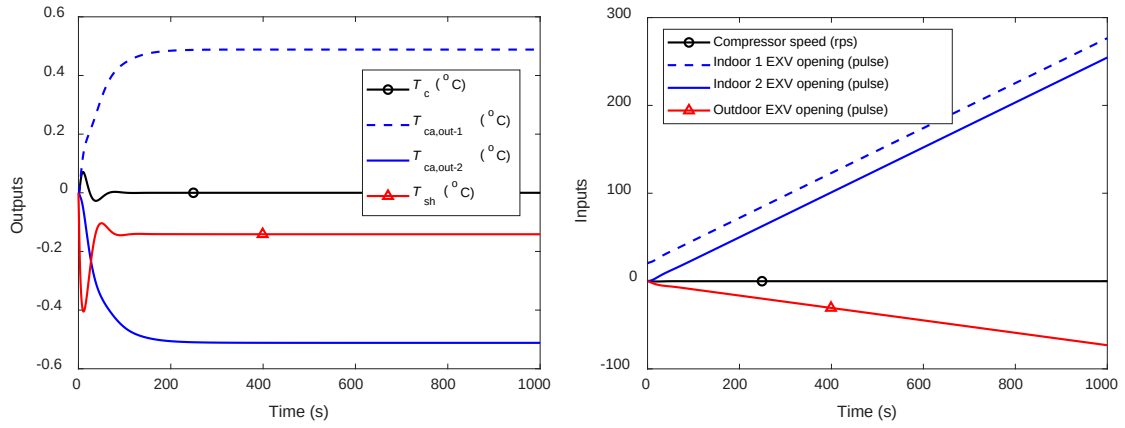


(a) Control objective $\mathbf{Y}$ = [0 1 0 0]

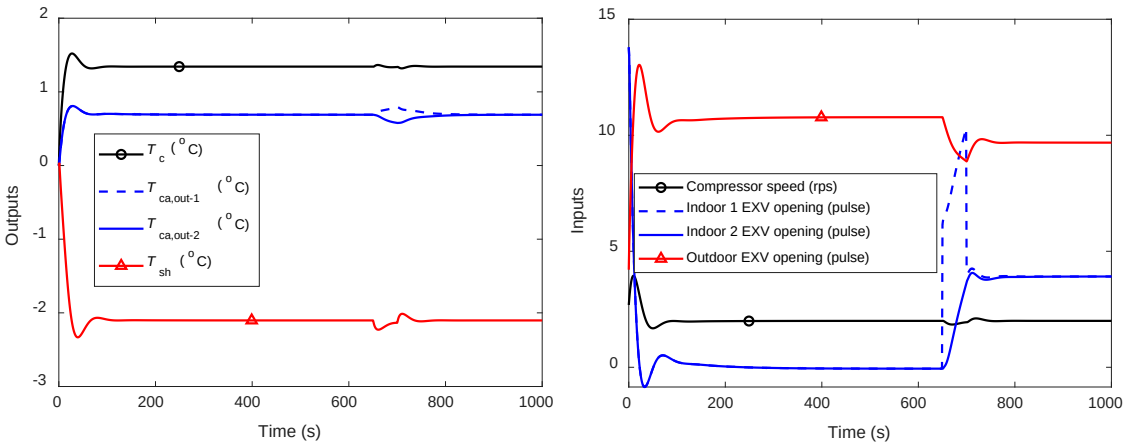


(b) Control objective $\mathbf{Y}$ is the linear combination of $\mathbf{G}_0$, Y = [1.3429 0.6896 0.6896 -2.1029]

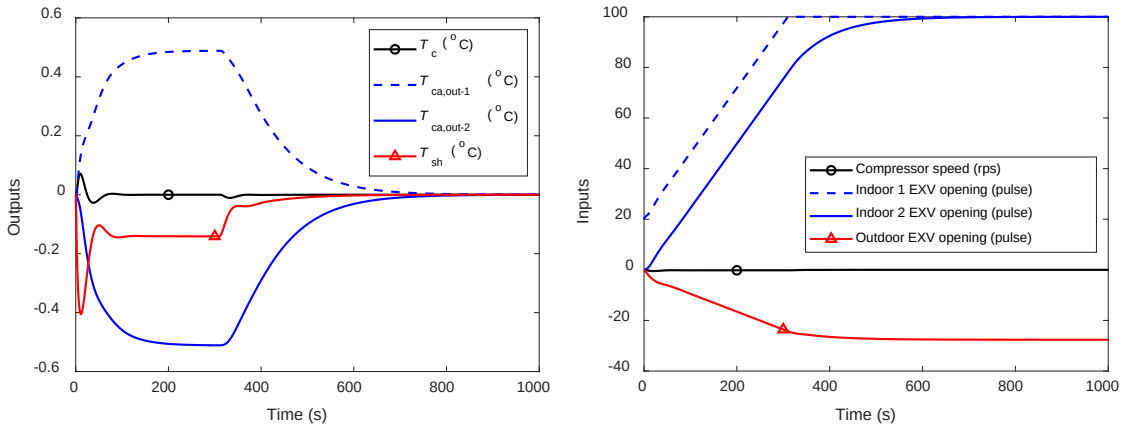


(c) Control objective **Y** = [0 1 0 0] with constrained indoor EXV opening strategy

Fig.9 Command-following performance with conventional control strategy

### 4.2.2 Control performance with the modified control strategy

A simulation controllability test of the modified control strategy was carried out under the same conditions as the conventional control strategy. Fig.10 (a) shows the command-following performance when control target **Y** = [0 1 0 0] is imposed from $t$ = 0 s. That is, the setpoint of supply air temperature of indoor unit 1 ($T_{ca\_out-1}$) increase by 1 °C, while setpoints of other three outputs remain unchanged. As can be seen, target settings of output variables were all successfully met. Control inputs, especially EXV openings, were rapidly stabilized. Thus, the control performance of multi-condenser heat pumps was essentially improved.

Fig.10 (b) shows another set of command-following performance, where control target **Y** is a linear combination of columns from the steady-state gain matrix $\mathbf{G}_0$. The change of setpoints for the four outputs represented by vector **Y** is introduced from 0 s. A small disturbance in the reference setting of $T_{ca,out-2}$ is introduced during the 651 – 700 s period, just same as that used in the controllability test of the conventional control strategy. The simulation results demonstrate that control targets for the outputs can be perfectly satisfied. Moreover, the indoor and outdoor EXVs stabilize at the same openings before and after the disturbance is introduced. Therefore, uncontrollability problems deriving from the conventional control strategy have been appropriately solved.

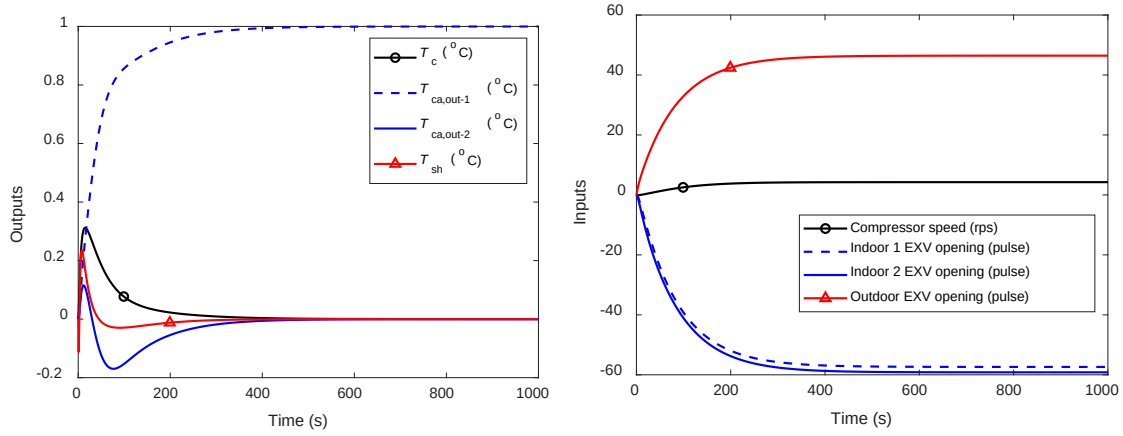


(a) Control objective **Y** = [0 1 0 0]

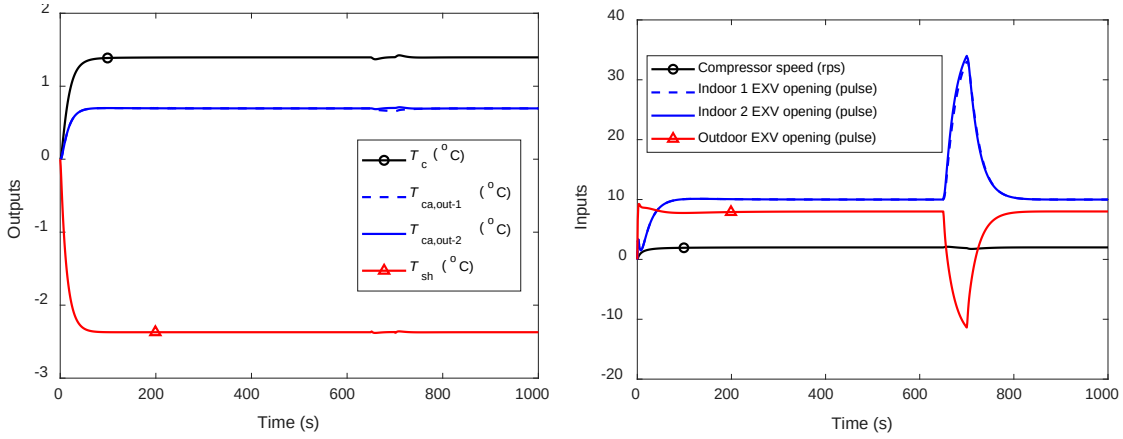


(b) Control objective **Y** being the linear combination of $\mathbf{G}_0$, Y= [1.3954, 0.6963, 0.6963, -2.3710]

Fig.10 Command-following performance using the modified control strategy

The above simulation command-following test verified findings from functional controllability analysis. For the case of multi-condenser heat pumps, it is possible to detect the uncontrollable problem just based on expertise on system operation characteristics. However, for more complex and counterintuitive cases, functional controllability analysis provides a general method to detect uncontrollable problems. To numerically analyze the functional controllability of a system, we should develop its dynamic model and calculate singular values at any frequency. A plant is functionally uncontrollable if and only if the minimum singular value at any frequency equals zero. By performing functional controllability analysis, we can find structural problems in control and obtain insight into the source of the problem, which is useful for further design changes.

# 5 Conclusions

The conventional heating control strategy for a multi-condenser heat pump is to have the indoor EXV openings control the subcooling or the supply air temperature of each indoor unit while the outdoor EXV opening controls the suction superheat. This study in-depth investigated the conventional control strategy and reach the main conclusions as follows.

The conventional strategy was found uncontrollable from detailed experimental investigations and theoretical proof. Specifically, it would result in unstable EXV openings and poor command-following performance.

A modified system design, in which a receiver located between the indoor EXVs and outdoor EXV was added, was proposed to solve the uncontrollable problem. The controllability of the modified system and control strategy was verified by simulations.

The methodology of functional controllability not only can solve the controllable problem of VRF system but also can be applied to the control design of different refrigeration and heat pump systems.

## Acknowledgement

The authors gratefully acknowledge the financial support of Research Institute for Sustainable Urban Development (RISUD) of the Hong Kong Polytechnic University.

## References

[1] T.N. Aynur, Variable refrigerant flow systems: A review, Energy and Buildings, 42 (2010) 1106-1112.
[2] R. Shah, A. Alleyne, C. Bullard, B. Rasmussen, P. Hrnjak, Dynamic modeling and control of single and multi-evaporator subcritical Vapor Compression Systems, 2003.
[3] W. Chen, X. Zhou, S. Deng, Development of control method and dynamic model for multi-evaporator air conditioners (MEAC), Energy Conversion and Management, 46 (2005) 451-465.
[4] M.S. Elliott, B.P. Rasmussen, Model-based predictive control of a multi-evaporator vapor compression cooling cycle, in: American Control Conference, Seattle, Washington, 2008, pp. 1463-1468.
[5] M.S. Elliott, B.P. Rasmussen, Decentralized model predictive control of a multi-evaporator air conditioning system, Control Engineering Practice, 21 (2013) 1665-1677.
[6] J.-L. Lin, T.J. Yeh, Control of multi-evaporator air-conditioning systems for flow distribution, Energy Conversion and Management, 50 (2009) 1529-1541.
[7] J.-L. Lin, T.J. Yeh, Mode switching control of dual-evaporator air-conditioning systems, Energy Conversion and Management, 50 (2009) 1542-1555.
[8] Q. Tu, K. Dong, D. Zou, Y. Lin, Experimental study on multi-split air conditioner with

digital scroll compressor, Applied Thermal Engineering, 31 (2011) 2449-2457.
[9] X. Xu, Y. Pan, S. Deng, L. Xia, M. Chan, Experimental study of a novel capacity control algorithm for a multi-evaporator air conditioning system, Applied Thermal Engineering, 50 (2013) 975-984.
[10] G.Y. Yun, J.H. Lee, H.J. Kim, Development and application of the load responsive control of the evaporating temperature in a VRF system for cooling energy savings, Energy and Buildings, 116 (2016) 638-645.
[11] K. Matsumoto, K. Ohno, S. Yamaguchi, K. Saito, Numerical analysis of control characteristics of variable refrigerant flow heat-pump systems focusing on the effect of expansion valve and indoor fan, International Journal of Refrigeration, 99 (2019) 440-452.
[12] Y. Tai, Control design for a multi-split air conditioning system, Journal of Taizhou Polytechnic College, 13 (2013) 75-78 (in Chinese).
[13] I.H. Lee, J.W. Choi, M.S. Kim, Studies on the heating capacity control of a multi-type heat pump system applying a multi-input multi-output (MIMO) method, International Journal of Refrigeration, 34 (2011) 416-428.
[14] G.Y. Yun, J.H. Lee, I. Kim, Dynamic target high pressure control of a VRF system for heating energy savings, Applied Thermal Engineering, 113 (2017) 1386-1395.
[15] J.W. Moon, Y.K. Yang, E.J. Choi, Y.J. Choi, K.-H. Lee, Y.-S. Kim, B.R. Park, Development of a control algorithm aiming at cost-effective operation of a VRF heating system, Applied Thermal Engineering, 149 (2019) 1522-1531.
[16] S. Skogestad, I. Postlethwaite, Multivariable feedback control : analysis and design, John Wiley, Chichester, England, 2005.
[17] H. Sun, G. Ding, H. Hu, T. Ren, G. Xia, G. Wu, A general simulation model for variable refrigerant flow multi-split air conditioning system based on graph theory, International Journal of Refrigeration, 82 (2017) 22-35.
[18] G. Kim, J. Lee, J. Park, S. Song, Flow visualization and noise measurement of R410A two-phase flow near electric expansion valve for heating cycle of multi-split air-source heat pump, Applied Thermal Engineering, 157 (2019) 113712.
[19] K. Sun, G. Li, H. Chen, J. Liu, J. Li, W. Hu, A novel efficient SVM-based fault diagnosis method for multi-split air conditioning system's refrigerant charge fault amount, Applied Thermal Engineering, 108 (2016) 989-998.
[20] Z. Li, B. Wang, X. Li, W. Shi, S. Zhang, Y. Liu, Simulation of recombined household multi-split variable refrigerant flow system with split-type air conditioners, Applied Thermal Engineering, 117 (2017) 343-354.
[21] Daikin, Maintenance handbook for VRV series: RUXYQ8-66AB, Daikin Air Conditioning Cooperation, Shanghai, 2014.
[22] S. Shao, J. Tu, W. Shi, X. Li, Q. Yan, Review of technology on multiple VRV air conditioning system with variable frequency control (in Chinese), Refrigeration and air

conditioning, 3 (2003) 6-10.
[23] W. Shi, B. Wang, S. Shao, Design of small capacity air conditioners and heat pumps (in Chinese), China Architecture & Building Press, Beijing, 2013.
[24] D. Kang, J.H. Jeong, B. Ryu, Heating performance of a VRF heat pump system incorporating double vapor injection in scroll compressor, International Journal of Refrigeration, 96 (2018) 50-62.
[25] B. Min, S. Na, T. Lee, S. Jang, H. Bae, C. Moon, G. Choi, Performance analysis of multi-split variable refrigerant flow (VRF) system with vapor-injection in cold season, International Journal of Refrigeration, 99 (2019) 419-428.
[26] J.P. Koeln, A.G. Alleyne, Optimal subcooling in vapor compression systems via extremum seeking control: Theory and experiments, International Journal of Refrigeration, 43 (2014) 14-25.
[27] H.H. Rosenbrock, State-Space and Multivariable Theory, Nelson, London, 1970.
[28] X.-D. He, Dynamic modeling and multivariable control of vapor compression cycles in air conditioning systems in: Massachusetts Institute of Technology, Massachusetts Institute of Technology, Boston, 1997.
[29] W.-J. Zhang, C.-L. Zhang, A generalized moving-boundary model for transient simulation of dry-expansion evaporators under larger disturbances, International Journal of Refrigeration, 29 (2006) 1119-1127.
[30] C.L. Zhang, Fundamentals of Vapor-Compression Refrigeration and Air-Conditioning System Modeling, Chemical Industry Press, Beijing, 2012.
[31] W.-J. Zhang, C.-L. Zhang, G.-L. Ding, On three forms of momentum equation in transient modeling of residential refrigeration systems, International Journal of Refrigeration, 32 (2009) 938-944.
[32] Q. Qi, S. Deng, Multivariable control-oriented modeling of a direct expansion (DX) air conditioning (A/C) system, International Journal of Refrigeration, 31 (2008) 841-849.
[33] G. Strang, Linear algebra and its applications, 4th ed., Thomson, Brooks/Cole, Belmont, CA, 2006.

# Appendix

## A.1 Governing equations of the condenser

Governing equations of the condenser include refrigerant mass conservation equation in the two-phase region, refrigerant and tube wall energy conservation equation in the desuperheating, two-phase and subcooling region. They are detailed as following.

$$
\begin{cases}
\left(\rho_{\mathrm{gc}}-\rho_{\mathrm{lc}}\right)A_{\mathrm{c}}\dot{L}_{\mathrm{c1}}+\left(\rho_{\mathrm{gc}}-\rho_{\mathrm{lc}}\right)\bar{\gamma}_{\mathrm{c}}A_{\mathrm{c}}\dot{L}_{\mathrm{c2}}+\left(\dfrac{\mathrm{d}\rho_{\mathrm{lc}}}{\mathrm{d}p_{\mathrm{c}}}\left(1-\bar{\gamma}_{\mathrm{c}}\right)+\dfrac{\mathrm{d}\rho_{\mathrm{gc}}}{\mathrm{d}p_{\mathrm{c}}}\bar{\gamma}_{\mathrm{c}}\right)A_{\mathrm{c}}L_{\mathrm{c2}}\dot{p}_{\mathrm{c}}=m_{\mathrm{ci}}-m_{\mathrm{co}} \\
\rho_{\mathrm{gc}}\dfrac{h_{\mathrm{d}}-h_{\mathrm{gc}}}{2}A_{\mathrm{c}}\dot{L}_{\mathrm{c1}}+\left(\dfrac{\rho_{\mathrm{gc}}}{2}\left(\dfrac{\mathrm{d}h_{\mathrm{gc}}}{\mathrm{d}p_{\mathrm{c}}}+\dfrac{\partial h_{\mathrm{d}}}{\partial p_{\mathrm{c}}}\right)-1\right)A_{\mathrm{c}}L_{\mathrm{c1}}\dot{p}_{\mathrm{c}}+\dfrac{\rho_{\mathrm{gc}}}{2}\dfrac{\partial h_{\mathrm{d}}}{\partial T_{\mathrm{d}}}A_{\mathrm{c}}L_{\mathrm{c1\text{-}a}}\dot{T}_{\mathrm{d}} \\
=m_{\mathrm{ci}}\left(h_{\mathrm{d}}-h_{\mathrm{gc}}\right)+\alpha_{\mathrm{c1}}\pi D_{\mathrm{c}}L_{\mathrm{c1}}\left(T_{\mathrm{cw1}}-\left(T_{\mathrm{d}}+T_{\mathrm{c}}\right)/2\right) \\
\left(\rho_{\mathrm{gc}}h_{\mathrm{gc}}-\rho_{\mathrm{lc}}h_{\mathrm{lc}}\right)A_{\mathrm{c}}\dot{L}_{\mathrm{c1}}+\left(\rho_{\mathrm{gc}}h_{\mathrm{gc}}-\rho_{\mathrm{lc}}h_{\mathrm{lc}}\right)\bar{\gamma}_{\mathrm{c}}A_{\mathrm{c}}\dot{L}_{\mathrm{c2}}+\left(\dfrac{\mathrm{d}\rho_{\mathrm{lc}}h_{\mathrm{lc}}}{\mathrm{d}p_{\mathrm{c}}}\left(1-\bar{\gamma}_{\mathrm{c}}\right)+\dfrac{\mathrm{d}\rho_{\mathrm{gc}}h_{\mathrm{gc}}}{\mathrm{d}p_{\mathrm{c}}}\bar{\gamma}_{\mathrm{c}}-1\right)A_{\mathrm{c}}L_{\mathrm{c2}}\dot{p}_{\mathrm{c}} \\
=m_{\mathrm{ci}}h_{\mathrm{gc}}-m_{\mathrm{co}}h_{\mathrm{lc}}+\alpha_{\mathrm{c2}}\pi D_{\mathrm{c}}L_{\mathrm{c2}}\left(T_{\mathrm{cw2}}-T_{\mathrm{c}}\right) \\
\rho_{\mathrm{lc}}\dfrac{h_{\mathrm{lc}}-h_{\mathrm{liq}}}{2}A_{\mathrm{c}}\dot{L}_{\mathrm{c1}}+\rho_{\mathrm{lc}}\dfrac{h_{\mathrm{lc}}-h_{\mathrm{liq}}}{2}A_{\mathrm{c}}\dot{L}_{\mathrm{c2}}+\left(\dfrac{\rho_{\mathrm{lc}}}{2}\left(\dfrac{\mathrm{d}h_{\mathrm{lc}}}{\mathrm{d}p_{\mathrm{c}}}+\dfrac{\partial h_{\mathrm{liq}}}{\partial p_{\mathrm{c}}}\right)-1\right)A_{\mathrm{c}}L_{\mathrm{c3}}\dot{p}_{\mathrm{c}}+\dfrac{\rho_{\mathrm{lc}}}{2}\dfrac{\partial h_{\mathrm{liq}}}{\partial T_{\mathrm{liq}}}A_{\mathrm{c}}L_{\mathrm{c3}}\dot{T}_{\mathrm{liq}} \\
=m_{\mathrm{co}}\left(h_{\mathrm{lc}}-h_{\mathrm{liq}}\right)+\alpha_{\mathrm{c3}}\pi DL_{\mathrm{c3}}\left(T_{\mathrm{cw3}}-\left(T_{\mathrm{c}}+T_{\mathrm{liq}}\right)/2\right) \\
\rho_{\mathrm{w}}c_{\mathrm{w}}A_{\mathrm{w}}\dfrac{L_{\mathrm{c1}}}{L_{\mathrm{c1}}+L_{\mathrm{c2}}}\left(T_{\mathrm{cw},1}-T_{\mathrm{cw},2}\right)\dot{L}_{\mathrm{c1}}+\rho_{\mathrm{w}}c_{\mathrm{w}}A_{\mathrm{w}}L_{\mathrm{c1}}\dot{T}_{\mathrm{cw1}} \\
=\alpha_{\mathrm{c1}}\pi D_{\mathrm{c}}L_{\mathrm{c1}}\left(\left(T_{\mathrm{d}}+T_{\mathrm{c}}\right)/2-T_{\mathrm{cw\,1}}\right)+\alpha_{\mathrm{co}}\pi D_{\mathrm{c}}L_{\mathrm{c1}}\left(T_{\mathrm{ca1}}-T_{\mathrm{cw1}}\right)/A_{\mathrm{r}} \\
\rho_{\mathrm{w}}c_{\mathrm{w}}A_{\mathrm{w}}\left(\dfrac{L_{\mathrm{c2}}T_{\mathrm{cw},1}+L_{\mathrm{c1}}T_{\mathrm{cw},2}}{L_{\mathrm{c1}}+L_{\mathrm{c2}}}-\dfrac{L_{\mathrm{c3}}T_{\mathrm{cw},2}+L_{\mathrm{c2}}T_{\mathrm{cw},3}}{L_{\mathrm{c2}}+L_{\mathrm{c3}}}\right)\dot{L}_{\mathrm{c1}}+\rho_{\mathrm{w}}c_{\mathrm{w}}A_{\mathrm{w}}\dfrac{L_{\mathrm{c2}}\left(T_{\mathrm{cw},2}-T_{\mathrm{cw},3}\right)}{L_{\mathrm{c2}}+L_{\mathrm{c3}}}\dot{L}_{\mathrm{c2}} \\
+\rho_{\mathrm{w}}c_{\mathrm{w}}A_{\mathrm{w}}L_{\mathrm{c2}}\dot{T}_{\mathrm{cw2}}=\alpha_{\mathrm{c2}}\pi D_{\mathrm{c}}L_{\mathrm{c2}}\left(T_{\mathrm{c}}-T_{\mathrm{cw2}}\right)+\alpha_{\mathrm{co}}\pi D_{\mathrm{c}}L_{\mathrm{c2}}\left(T_{\mathrm{ca2}}-T_{\mathrm{cw2}}\right)/A_{\mathrm{r}} \\
\rho_{\mathrm{w}}c_{\mathrm{w}}A_{\mathrm{w}}\dfrac{L_{\mathrm{c3}}\left(T_{\mathrm{cw},2}-T_{\mathrm{cw},3}\right)}{L_{\mathrm{c2}}+L_{\mathrm{c3}}}\dot{L}_{\mathrm{c1}}+\rho_{\mathrm{w}}c_{\mathrm{w}}A_{\mathrm{w}}\dfrac{L_{\mathrm{c3}}\left(T_{\mathrm{cw},2}-T_{\mathrm{cw},3}\right)}{L_{\mathrm{c2}}+L_{\mathrm{c3}}}\dot{L}_{\mathrm{c2}}+\rho_{\mathrm{w}}c_{\mathrm{w}}A_{\mathrm{w}}L_{\mathrm{c3}}\dot{T}_{\mathrm{cw3}} \\
=\alpha_{\mathrm{c3}}\pi D_{\mathrm{c}}L_{\mathrm{c3}}\left(\left(T_{\mathrm{c}}+T_{\mathrm{liq}}\right)/2-T_{\mathrm{cw3}}\right)+\alpha_{\mathrm{co}}\pi D_{\mathrm{c}}L_{\mathrm{c3}}\left(T_{\mathrm{ca3}}-T_{\mathrm{cw3}}\right)/A_{\mathrm{r}}
\end{cases}
\tag{34}
$$

## A.2 Expressions of *G* (X, U)

The nonlinear expression *G* (**X**, **U**) and its linearization are given by the following equations

$$
\begin{aligned}
&\delta G_{1}=\delta\left(m_{\mathrm{ei}}h_{\mathrm{ei}}-m_{\mathrm{eo}}h_{\mathrm{ge}}+\alpha_{\mathrm{e1}}\pi D_{\mathrm{e}}L_{\mathrm{e1}}\left(T_{\mathrm{ew1}}-T_{\mathrm{e}}\right)\right) \\
&=\left(\delta m_{\mathrm{d}}\cdot h_{\mathrm{ei}}+m_{\mathrm{d}}\delta h_{\mathrm{ei}}\right)-\left(\delta m_{\mathrm{comp}}\cdot h_{\mathrm{ge}}+m_{\mathrm{comp}}\delta h_{\mathrm{ge}}\right)+\delta Q_{\mathrm{e1}} \\
&=\left(k_{\mathrm{m\text{-}d}}h_{\mathrm{ei}}+k_{\mathrm{h\text{-}ei}}m_{\mathrm{d}}-k_{\mathrm{m\text{-}comp}}h_{\mathrm{ge}}-k_{\mathrm{h\text{-}ge}}m_{\mathrm{comp}}+k_{\mathrm{Qe1}}\right)\delta\begin{pmatrix}\mathbf{X} & \mathbf{U}\end{pmatrix}^{\mathrm{T}}
\end{aligned}
\tag{35}
$$

Where *k* represents partial derivatives of the subscript variable with respect to the state variables and input variables.

$$\begin{aligned}\delta G_2 &= \delta\left(m_{\text{eint}}\left(h_{\text{ge}}-h_{\text{s}}\right)+\alpha_{\text{e2}}\pi D_{\text{e}}L_{\text{e2}}\left(T_{\text{ew2}}-\left(T_{\text{e}}+T_{\text{s}}\right)/2\right)\right)\\ &= \delta m_{\text{comp}}\left(h_{\text{ge}}-h_{\text{s}}\right)+m_{\text{comp}}\left(\delta h_{\text{ge}}-\delta h_{\text{s}}\right)+\delta\left(\alpha_{\text{e2}}\pi D_{\text{e}}L_{\text{e2}}\left(T_{\text{ew2}}-\left(T_{\text{e}}+T_{\text{s}}\right)/2\right)\right)\\ &= \left(k_{\text{m-comp}}\left(h_{\text{ge}}-h_{\text{s}}\right)+k_{\text{h-ge}}m_{\text{comp}}-k_{\text{h-s}}m_{\text{comp}}+k_{Q\text{e2}}\right)\delta\left(\mathbf{X}\quad\mathbf{U}\right)^{\text{T}}\end{aligned} \tag{36}$$

$$\begin{aligned}\delta G_3 &= \delta\left(\alpha_{\text{e1}}\pi D_{\text{e}}L_{\text{e1}}\left(T_{\text{e}}-T_{\text{ew1}}\right)+\alpha_{\text{eo}}\pi D_{\text{e}}L_{\text{e1}}\left(T_{\text{ea1}}-T_{\text{ew1}}\right)/A_{\text{r}}\right)\\ &= \left(-k_{Q\text{e1}}+k_{Q\text{ea1}}\right)\delta\left(\mathbf{X}\quad\mathbf{U}\right)^{\text{T}}\end{aligned} \tag{37}$$

$$\begin{aligned}\delta G_4 &= \delta\left(\alpha_{\text{e2}}\pi D_{\text{e}}L_{\text{e2}}\left(\left(T_{\text{e}}+T_{\text{s}}\right)/2-T_{\text{ew, 2}}\right)+\alpha_{\text{eo}}\pi D_{\text{e}}L_{\text{e2}}\left(T_{\text{ea2}}-T_{\text{ew2}}\right)/A_{\text{r}}\right)\\ &= \left(-k_{Q\text{e2}}+k_{Q\text{ea2}}\right)\delta\left(\mathbf{X}\quad\mathbf{U}\right)^{\text{T}}\end{aligned} \tag{38}$$

$$\begin{aligned}\delta G_5 &= \delta\left(m_{\text{comp}}\left(h_{\text{s}}-h_{\text{d}}\right)+W_{\text{comp}}-\alpha_{\text{comp}}A_{\text{comp}}\left(T_{\text{d}}-T_{\text{amb}}\right)-\varepsilon\sigma A_{\text{comp}}\left(T_{\text{d}}^{\ 4}-T_{\text{amb}}^{\ 4}\right)\right)\\ &= \delta m_{\text{comp}}\left(h_{\text{s}}-h_{\text{d}}\right)+m_{\text{comp}}\left(\delta h_{\text{s}}-\delta h_{\text{d}}\right)+\delta W_{\text{comp}}+\delta Q_{\text{comp}}\\ &= \left(k_{\text{m-comp}}\left(h_{\text{s}}-h_{\text{d}}\right)+k_{\text{h-s}}m_{\text{comp}}-k_{\text{h-d}}m_{\text{comp}}+k_{\text{w}-\text{comp}}+k_{Q-\text{comp}}\right)\delta\left(\mathbf{X}\quad\mathbf{U}\right)^{\text{T}}\end{aligned} \tag{39}$$

$$\delta G_6 = \delta\left(m_{\text{ci-1}}-m_{\text{co-1}}\right)=\left(k_{\text{m}-\text{ci1}}-k_{\text{m}-\text{co1}}\right)\delta\left(\mathbf{X}\quad\mathbf{U}\right)^{\text{T}} \tag{40}$$

$$\begin{aligned}\delta G_7 &= \delta\left(m_{\text{ci-1}}\left(h_{\text{d}}-h_{\text{gc}}\right)+\alpha_{\text{c1}}\pi D_{\text{c}}L_{\text{c1-1}}\left(T_{\text{cw1-1}}-\left(T_{\text{d}}+T_{\text{c1}}\right)/2\right)\right)\\ &= \delta m_{\text{ci-1}}\left(h_{\text{d}}-h_{\text{gc}}\right)+m_{\text{ci-1}}\left(\delta h_{\text{d}}-\delta h_{\text{gc}}\right)+\delta Q_{\text{c1-1}}\\ &= \left(k_{\text{m-ci1}}\left(h_{\text{d}}-h_{\text{gc}}\right)+k_{\text{h-d}}m_{\text{ci-1}}-k_{\text{h-gc}}m_{\text{ci-1}}+k_{Q\text{c1}-1}\right)\delta\left(\mathbf{X}\quad\mathbf{U}\right)^{\text{T}}\end{aligned} \tag{41}$$

$$\begin{aligned}\delta G_8 &= \delta\left(m_{\text{ci-1}}h_{\text{gc}}-m_{\text{co-1}}h_{\text{lc}}+\alpha_{\text{c2}}\pi D_{\text{c}}L_{\text{c2}-1}\left(T_{\text{cw2-1}}-T_{\text{c1}}\right)\right)\\ &= \left(\delta m_{\text{ci-1}}\cdot h_{\text{gc}}+m_{\text{ci-1}}\delta h_{\text{gc}}\right)-\left(\delta m_{\text{co-1}}\cdot h_{\text{lc}}+m_{\text{co-1}}\delta h_{\text{lc}}\right)+\delta Q_{\text{c2-1}}\\ &= \left(k_{\text{m-ci1}}h_{\text{gc}}+k_{\text{h-gc}}m_{\text{ci-1}}-k_{\text{m-co1}}h_{\text{lc-1}}-k_{\text{h-lc-1}}m_{\text{co-1}}+k_{Q\text{c2}-1}\right)\delta\left(\mathbf{X}\quad\mathbf{U}\right)^{\text{T}}\end{aligned} \tag{42}$$

$$\begin{aligned}\delta G_9 &= \delta\left(m_{\text{co-1}}\left(h_{\text{lc-1}}-h_{\text{liq-1}}\right)+\alpha_{\text{c3}}\pi DL_{\text{c3-1}}\left(T_{\text{cw3-1}}-\left(T_{\text{c1}}+T_{\text{liq-1}}\right)/2\right)\right)\\ &= \delta m_{\text{co-1}}\left(h_{\text{lc-1}}-h_{\text{liq-1}}\right)+m_{\text{co-1}}\left(\delta h_{\text{lc-1}}-\delta h_{\text{liq-1}}\right)+\delta Q_{\text{c3-1}}\\ &= \left(k_{\text{m-co1}}\left(h_{\text{lc-1}}-h_{\text{liq-1}}\right)+k_{\text{h-lc-1}}m_{\text{co-1}}-k_{\text{h-liq-1}}m_{\text{co-1}}+k_{Q\text{c3}-1}\right)\delta\left(\mathbf{X}\quad\mathbf{U}\right)^{\text{T}}\end{aligned} \tag{43}$$

$$\begin{aligned}\delta G_{10} &= \delta\left(\alpha_{\text{c1}}\pi D_{\text{c}}L_{\text{c1-1}}\left(\left(T_{\text{d}}+T_{\text{c1}}\right)/2-T_{\text{cw1-1}}\right)+\alpha_{\text{co}}\pi D_{\text{c}}L_{\text{c1}-1}\left(T_{\text{ca1-1}}-T_{\text{cw1-1}}\right)/A_{\text{r}}\right)\\ &= \left(-k_{Q\text{c1-1}}+k_{Q\text{ca1-1}}\right)\delta\left(\mathbf{X}\quad\mathbf{U}\right)^{\text{T}}\end{aligned} \tag{44}$$

$$\begin{aligned}\delta G_{11} &= \delta\left(\alpha_{\text{c2}}\pi D_{\text{c}}L_{\text{c2}-1}\left(T_{\text{c1}}-T_{\text{cw2-1}}\right)+\alpha_{\text{co}}\pi D_{\text{c}}L_{\text{c2}-1}\left(T_{\text{ca2-1}}-T_{\text{cw2-1}}\right)/A_{\text{r}}\right)\\ &= \left(-k_{Q\text{c2-1}}+k_{Q\text{ca2-1}}\right)\delta\left(\mathbf{X}\quad\mathbf{U}\right)^{\text{T}}\end{aligned} \tag{45}$$

$$\begin{aligned}\delta G_{12} &= \delta\left(\alpha_{\text{c3}}\pi D_{\text{c}}L_{\text{c3-1}}\left(\left(T_{\text{c1}}+T_{\text{liq-1}}\right)/2-T_{\text{cw3-1}}\right)+\alpha_{\text{co}}\pi D_{\text{c}}L_{\text{c3-1}}\left(T_{\text{ca3-1}}-T_{\text{cw3-1}}\right)/A_{\text{r}}\right)\\ &= \left(-k_{Q\text{c3-1}}+k_{Q\text{ca3-1}}\right)\delta\left(\mathbf{X}\quad\mathbf{U}\right)^{\text{T}}\end{aligned} \tag{46}$$

In the above equations, Eqs. (35) through (38), i.e., $\delta G_1$ to $\delta G_4$, correspond to governing

equations of the evaporator. Eq. (39), that is, $\delta G_5$ is the right side in the energy balance equation of the compressor. Likewise, Eqs. (40) through (46), i.e., $\delta G_6$ to $\delta G_{12}$, are related with mass and energy conservation equations of the first condenser. Governing equations of the other condenser can be simply obtained by replacing subscript “1” in Eqs. (40) through (46) with subscript “2”.